Accepted Manuscript

Targeting G-quadruplex DNA structures in the telomere and oncogene promoter regions by benzimidazole–carbazole ligands

Mangesh H. Kaulage, Basudeb Maji, Sanjeev Pasadi, Asfa Ali, Santanu Bhattacharya, Kalappa Muniyappa

PII: S0223-5234(18)30113-2

DOI: 10.1016/j.ejmech.2018.01.091

Reference: EJMECH 10168

To appear in: *European Journal of Medicinal Chemistry*

Received Date: 17 November 2017

Revised Date: 17 January 2018

Accepted Date: 27 January 2018

Please cite this article as: M.H. Kaulage, B. Maji, S. Pasadi, A. Ali, S. Bhattacharya, K. Muniyappa, Targeting G-quadruplex DNA structures in the telomere and oncogene promoter regions by benzimidazole–carbazole ligands, *European Journal of Medicinal Chemistry* (2018), doi: 10.1016/j.ejmech.2018.01.091.

Targeting G-quadruplex DNA structures in the telomere and oncogene promoter regions by benzimidazole–carbazole ligands

Mangesh H. Kaulage [a,b,1], Basudeb Maji [b,1], Sanjeev Pasadi [a], Asfa Ali [b], Santanu Bhattacharya [b*] and Kalappa Muniyappa [a*]

[a]Department of Biochemistry, Indian Institute of Science, Bangalore 560012, India.

[b]Department of Organic Chemistry, Indian Institute of Science, Bangalore 560012, India.

[1]These authors contributed equally to this work.

[*]To whom correspondence should be addressed: Email: kmbc@iisc.ac.in or sb@iisc.ac.in

Graphical abstract

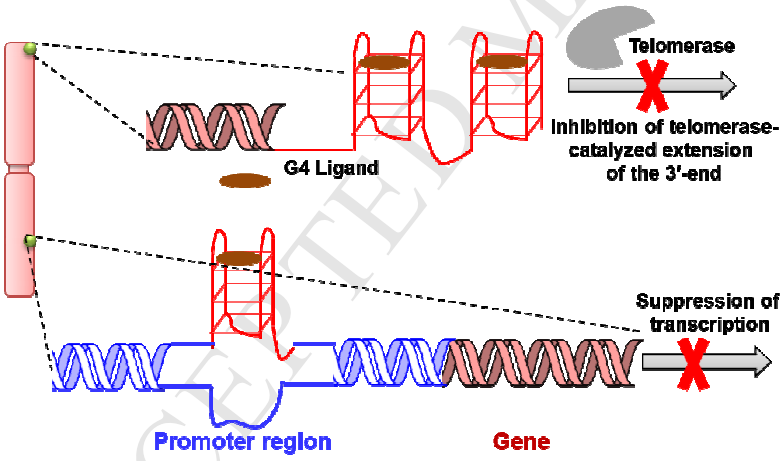

Highlights

- Benzimidazole-carbazole ligands stabilize promoter and telomere G4 DNA
- Benzimidazole-carbazole ligands stabilize parallel topology of G4 DNA
- Ligand-mediated G4 DNA stabilization inhibits extension of 3' end of telomere
- Ligand-mediated G4 DNA stabilization at the promoters suppresses gene expression

Abstract

Recent studies support the idea that G-quadruplex structures in the promoter regions of oncogenes and telomere DNA can serve as potential therapeutic targets in the treatment of cancer. Accordingly, several different types of organic small molecules that stabilize G-quadruplex structures and inhibit telomerase activity have been discerned. Here, we describe the binding of benzimidazole-carbazole ligands to G-quadruplex structures formed in G-rich DNA sequences containing the promoter regions of human *c-MYC, c-KIT1, c-KIT2, VEGF* and *BCL2* proto-oncogenes. The fluorescence spectroscopic data indicate that benzimidazole-carbazole ligands bind and preferentially stabilize the parallel topology of G-quadruplexes in the promoter region of oncogenes. The molecular docking studies provide insights into the mode and extent of binding of this class of ligands to the G-quadruplexes formed in oncogene promoters. The high stability of these G-quadruplex structures was validated by thermal denaturation and telomerase-catalyzed extension of the 3' end. Notably, benzimidazole-carbazole ligands suppress the expression of oncogenes in cancer cells in a dose-dependent manner. We anticipate that benzimidazole-carbazole ligands, by virtue of their ability to stabilize G-quadruplex structures in

the promoter regions of oncogenes, might reduce the risk of cancer through the loss of function in the proteins encoded by these genes.

Keywords: Oncogenes, G-quadruplex DNA, benzimidazole–carbazole conjugates, thiazole orange, fluorescence intercalator displacement, polymerase stop assay, transcriptional regulation.

1. Introduction

The human genome contains highly repetitive sequences: among them, the most polymorphic are the G-rich sequences, which readily fold into a variety of G-quadruplex structures [1]. A typical G-quadruplex comprises of a planar cyclic array of four guanine residues held together by Hoogsteen hydrogen bonds [1]. By stacking on top of each other, these tetrads produce a right-handed quadruple helical structure. The G-rich sequences give rise to diverse G-quadruplex structures by folding inter- or intra-molecularly and can form hybrid-type mixed parallel/antiparallel G-strands [1-3]. The intramolecular G-quadruplex structures can adopt diverse topologies; depending on the orientation of strands, size/sequence of loops, glycosidic torsion angles, and type of metal ions [1-3]. The computational studies and high-throughput sequencing have revealed that approximately 716310 distinct G-quadruplex forming sequences exist in the human genome [4, 5].

A significant body of work has also shown that G-quadruplex forming sequences are not randomly distributed throughout the genome, but tend to cluster in specific regions. The non-random distribution of G-quadruplex forming sequences and their evolutionary conservation in genomes posit that these sequences may be associated with a wide range of fundamental biological processes [4, 6, 7]. The most common form of DNA in cells is the B-form, in which

G/C base pairing precludes the formation of G-quadruplex structures. However, the guanines within a G/C-rich region can fold into G-quadruplex structures as a consequence of transient strand separation during the processes of transcription, replication and recombination [8, 9]. The research activity in the area of G-quadruplex structures has hugely expanded in the past decade due to their existence at biologically relevant loci under physiological conditions and their potential druggability in human cells [10-12].

The telomeres protect chromosomes from degradation and genomic instability; they also regulate telomerase activity [13, 14]. Telomerase is a reverse transcriptase that plays a key role in telomere length homeostasis by adding TTAGGG repeats to the ends of chromosomes [15, 16]. For optimal telomerase activity, unfolded telomeric G-rich single strands are a necessity; on the other hand, folding of this overhang into a G-quadruplex structure inhibits telomere elongation by telomerase. Given the fact that telomerase is overexpressed in a majority of human cancer cells, it has emerged as a potential target in the development of anti-cancer drugs [17]. Among several different approaches to telomerase inhibition, the stabilization of G-quadruplexes by small molecules has received much attention [18]. As human telomeric single-stranded DNA (ssDNA) folds into a variety of intramolecular G-quadruplex structures [19-23], the structural features that are considered during the development of ligands include the G-tetrad surface, discrete grooves resulting from combinations of *syn*- and *anti*- deoxyguanosine conformations, a central channel with a negative charge and motifs within the flexible loop regions [24]. Owing to their potential roles in disease pathology, several hundreds of small molecules that interact with and stabilize telomeric G-quadruplex structures have been reported in literature [25].

Previous analyses using bioinformatics tools have revealed that G-quadruplex DNA motifs are embedded within the promoters of human oncogenes as well in several genes that encode

transcription factors, but are under-represented in the promoters of housekeeping genes and tumor suppressor genes [24, 26]. A number of studies have provided persuasive evidence supporting functional roles of the promoter G-quadruplexes of various human genes such as *INS* [27], *c-MYC* [28], *VEGF* [29], *HIF-1α* [30], *BCL-2* [31], *MtCK* [32], *KRAS* [33], *c-KIT* [34], *RET* [35], *PDGF-A* [36] and *ACC1* [37] and also their potential druggability [1, 18, 38]. Several classes of small molecules that bind and stabilize telomeric G-quadruplex structures have been reported [25, 39, 40]. Most of the reported ligands have a planar aromatic surface and interact with the external surface of the G-quartet by π-stacking interactions. Along with this selectivity and affinity of a ligand can be enhanced by the electrostatic as well as H-bonding interactions of the neutral/cationic side chain with the grooves/loops of the quadruplex structure [39, 41].

In previous research works, a variety of experimental techniques have revealed that benzimidazole–carbazole ligands selectively bind and stabilize telomeric G-quadruplex structures, inhibit telomerase activity and proliferation of human cancer cells [42, 43]. Additionally, these ligands were found to induce topological conversion from non-parallel to parallel forms in human telomeric G-quadruplex structures [42, 43]. In this study, we demonstrate the ability of benzimidazole-carbazole ligands to bind, stabilize and target G-quadruplex structures formed at telomeres and in the promoter regions of human *c-MYC*, *c-KIT1*, *c-KIT2, VEGF* and *BCL2* proto-oncogenes. The data presented here suggest that benzimidazole-carbazole ligands can inhibit telomerase-catalyzed extension of the 3' end [42]. The biological evidence that these ligands have important physiological consequences are presented: they suppress the expression of oncogenes in human cells thus indicating cellular relevance to oncogene promoter G-quadruplexes and potential to reduce the risk of cancer.

2. Results and Discussion

2.1. Ligands used in this study

The benzimidazole scaffolds are a valuable class of heterocyclic compounds that have many applications in the pharmaceutical industry. The benzimidazole containing compounds interact with various cellular targets (DNA being the primary target) and elicit a variety of cellular responses. Owing to their planarity, benzimidazole derivatives have the potential to interact with DNA via the intercalation binding mode [44-46]. Another class of compounds, which contain the bis-benzimidazole group (for example: Hoechst 33342 and Hoechst 33258) interact through the minor groove of duplex DNA [47, 48]. The benzimidazole-transition metal ion conjugates also interact with DNA. For example, benzimidazole-Cu^{2+} complexes intercalate into duplex DNA [49]. The binding activity of benzimidazole moiety (containing groove binders) is also studied with respect to their interaction with G-quadruplex DNA [50].

The compounds containing a carbazole moiety express a wide range of pharmacological activities including anticancer, antiviral, antifungal, anticoagulant, antiparasitic, analgesic, anticonvulsant, antiulcer and antihypertensive activities [51-55]. The chemistry and biology of carbazoles have attracted great interest in the context of their use in the synthesis of DNA binders due to their desirable electronic structures and large π-conjugated surface. In addition, various functional groups can be attached to a structurally rigid carbazolyl ring. The ligands containing carbazole moiety bind to the minor groove of A/T-rich sequences and also interact by intercalation as they contain a flat chromophore [56]. The research stimulated by the attractive properties of carbazoles has led to the synthesis of carbazole derivatives that recognize and stabilize a variety of G-quadruplex DNA structures [42, 43, 49, 56-60].

In previous research work, benzimidazole-carbazole conjugates were shown to selectively stabilize telomeric G-quadruplex DNA over duplex DNA [42]. These ligands possess carbazole as a central pharmacophore with varying number of flanking benzimidazole moieties and they preferentially bind to telomeric G-quadruplex DNA over duplex DNA. In this study, the ability of benzimidazole-carbazole conjugates to bind the G-quadruplex structures formed by G-rich DNA sequences (Table 1) in the promoter region of human *c-MYC, c-KIT1, c-KIT2, VEGF* and *BCL2* proto-oncogenes was investigated. Five benzimidazole-carbazole conjugate ligands were used (Fig. 1), of which the synthesis of ligand **2** and **4** have been reported previously [42]; newly synthesized ligands **1**, **3** and **5** were included to widen the pharmacological scope. The strategy employed in the synthesis of ligand **1** was based on the observation that carbazole-benzimidazole pharmacophore efficiently binds to and stabilizes telomeric G-quadruplex DNA [42]. While protonatable hydroxyethyl piperazine moieties in ligand **1** can electrostatically interact with negatively charged phosphodiester backbone, the hydroxyl moieties can function as hydrogen bond donor. Further, ligand **2** has three protonatable piperazine or morpholine moieties which can impart electrostatic interactions and ligand **3** contains an extra hard positive charge that might facilitate ligand-DNA interaction. Both ligand **2** and **3** are devoid of the hydroxyethyl group and can disable the H-bond donor property. In the case of ligands **4** and **5**, the hydroxyethyl group along with three protonatable moieties, either N-methyl-piperazine or dimethylamine, was added. Thus, keeping the carbazole-bis-benzimidaole central pharmacophore common, the peripheral functional groups were varied to study their effect on G-quadruplex binding efficacy and changes in their specificity towards different topological structures.

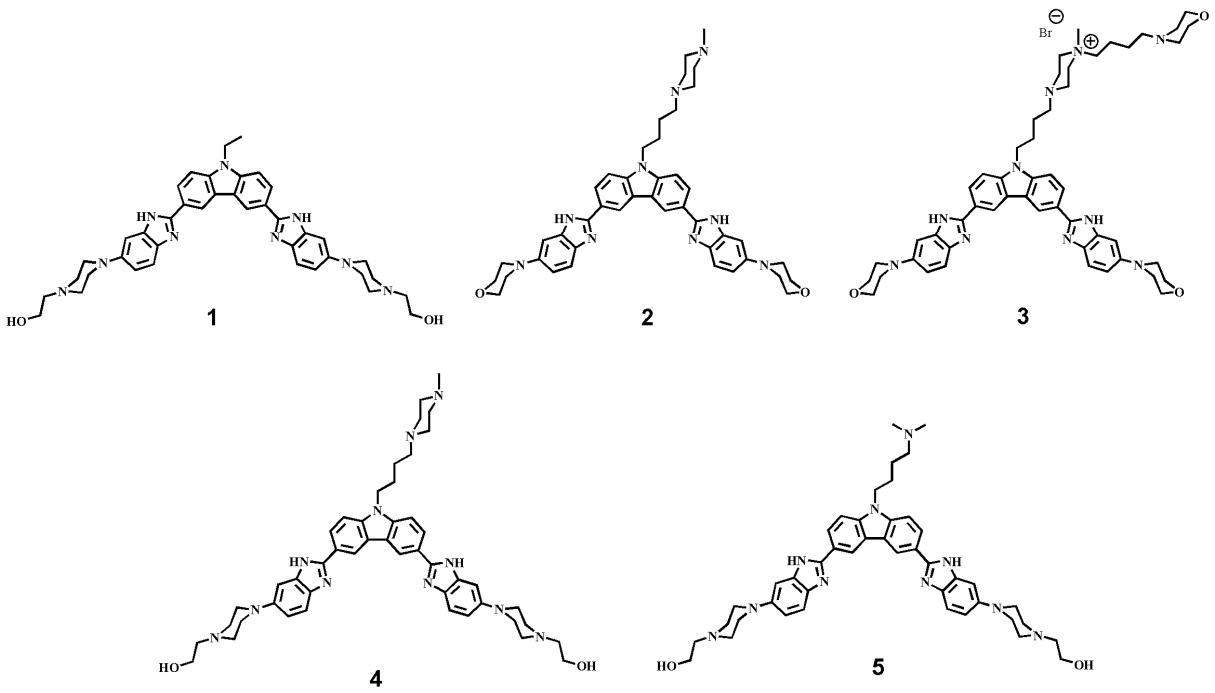

Figure. 1. Structure of benzimidazole–carbazole conjugates used in this study.

Table 1. Telomeric and oncogene promoter oligonucleotide sequences used in this study.

Promoter	5'<-----Sequence----->3'
C-Myc	TGGGGAGGGTGGGGAGGGTGGGGAAGG
VEGF	CGGGGCGGGCCGGGGGCGGGGT
Telomere	TTAGGGTTAGGGTTAGGGTTAGGG
c-Kit	AGGGAGGGCGCTGGGAGGAGGG
c-Kit-2	CGGGCGGGCGCGAGGGAGGGG
BCL2	AGGGGCGGGCGCGGGAGGAAGGGGGCGGGAGCGGGGCTG

2.2. Fluorescence emission spectral titrations

To investigate the ability of different benzimidazole–carbazole conjugates (ligands **1**-**5**) to bind G-quadruplexes formed by the telomere and oncogene promoter sequences (*c-MYC*, *c-KIT1*, *c-KIT2, VEGF* and *BCL2*), fluorescence titration experiments were carried out. In these

experiments, a fixed concentration of a specified ligand was titrated against increasing concentrations of the indicated G-quadruplex. All the ligands exhibited very weak emissions after excitation at 330 nm, which could be due to the collisional quenching of the singlet-excited state by polar water molecules. The ligand **1** alone displayed an extremely weak fluorescence emission (Fig. 2A). The addition of increasing concentrations of telomere G-quadruplex resulted in a substantially enhanced emission (maximum at 462 nm). In parallel, the ability of ligand **1** to bind oncogene promoter (*c-MYC, BCL2, c-KIT1, c-KIT2, and VEGF*) G-quadruplexes was measured. The fluorescence intensity increased significantly as the ligand was titrated with each of the G-quadruplex DNA substrates derived from the indicated oncogene promoter G-rich sequences (Fig. 2B-2F).

Similarly, fluorescence titration experiments were performed with ligands **2-5** and the results corroborated the effect of ligand **1**. The influence of ligands **2-5** on the fluorescence emission spectra was evident from the differences in emission profiles upon addition of increasing concentrations of the oncogene promoter G-quadruplex DNA, which was followed by saturation for each ligand (supplementary Fig. S1-S4). The enhancement in fluorescence intensity suggests that the ligands encounter an entirely hydrophobic environment upon binding, which in turn results in the retention of their intrinsic fluorescence emissions. Collectively, these fluorescence titration measurements support the idea that benzimidazole-carbazole conjugates interact with both telomere and oncogene promoter (*c-MYC, c-KIT1, c-KIT2, VEGF, and BCL2*) G-quadruplexes.

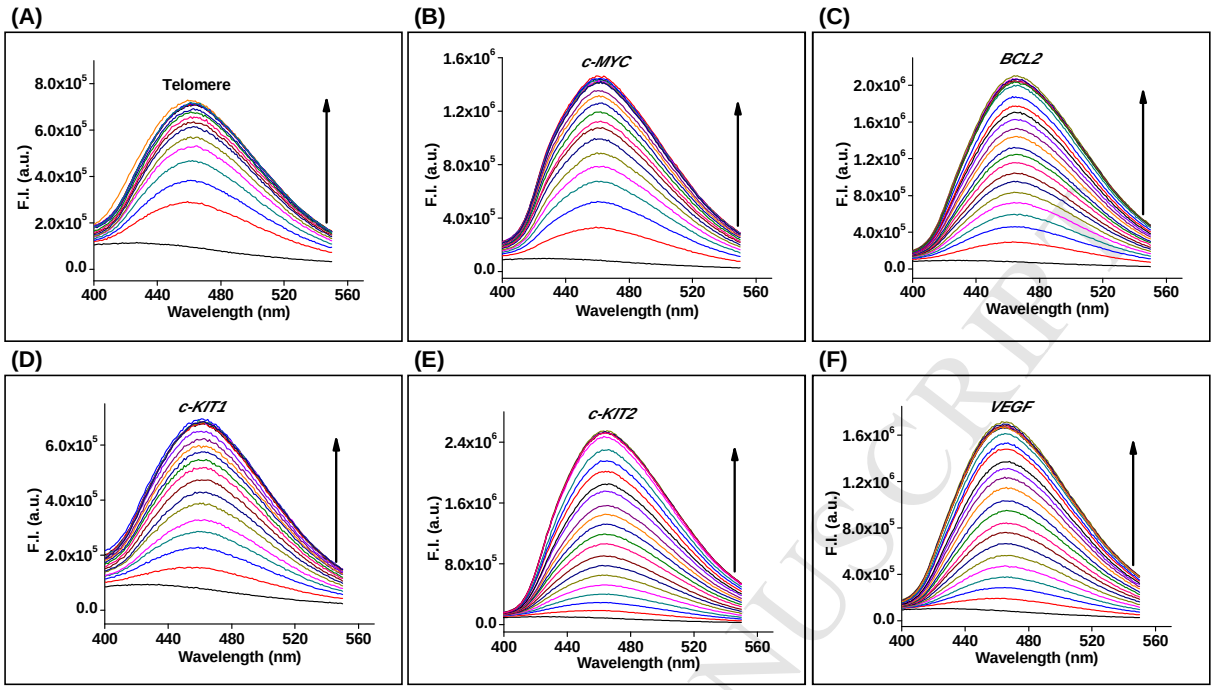

Figure. 2. Interaction of ligand **1** with different G-quadruplexes. The reaction mixtures contained a fixed amount (0.6 μM) of the indicated ligand in 10 mM Tris-HCl buffer (pH 7.4) with 100 mM KCl, 0.1 mM EDTA and increasing concentration of the specified G-quadruplex (as indicated in each panel). The fluorescence spectral tracings were obtained at each time point after the addition of an aliquot of G-quadruplex (0.15 μM). Panels A, B, C, D and E corresponds to telomeric, *c-MYC*, *BCL2*, *c-KIT1*, *c-KIT2* and *VEGF* G-quadruplex substrates, respectively. The vertical arrow represents relative increase in fluorescence intensity following addition of the specified G-quadruplex.

2.3. Effect of benzimidazole-carbazole conjugates on the conformation of G-quadruplexes

The foregoing studies indicated that benzimidazole-carbazole conjugates interact with telomere and oncogene promoter G-quadruplexes. Given the fact that G-quadruplexes can adopt various folding topologies [1-2,6-7], we sought to assess the effect of benzimidazole-carbazole

conjugates on the topology of oncogene promoter G-quadruplexes. Far-UV CD spectroscopy has been extensively used to monitor the different conformations of G-quadruplex structures in solution [61]. Thus, CD spectroscopy was employed in the current study to investigate the effect of different benzimidazole-carbazole ligands on the conformation of G-quadruplexes.

The reaction mixtures (in 10 mM Tris-HCl buffer, pH 7.4, containing 5 µM G-quadruplex DNA, 100 mM KCl and 0.1 mM EDTA; with or without different ligands) were heated at 95 °C for 5 min followed by slow cooling to room temperature. Then the spectra were recorded in the absence or presence of the indicated ligands. The *c-MYC, c-KIT1, c-KIT2* and *VEGF* promoter G-rich sequences consistently folded into parallel-stranded while the telomere and *BCL2* sequences folded into hybrid-type mixed parallel/antiparallel G-strands. The addition of ligand **1**, **4** or **5** to the G-quadruplex samples led to a structural inversion from the K^+ stabilized hybrid-type mixed parallel/antiparallel G-quadruplex to a stable telomere parallel-stranded G-quadruplex. The positive peaks at 288 nm and 267 nm merged to produce a positive peak at 264 nm and a negative peak at 241 nm, indicating the formation of parallel-stranded G4 DNA (Fig. 3A).

The telomeric G-rich sequence folds into a hybrid structure under physiological conditions; at the same time, it folds into a parallel-stranded conformation under molecular crowding conditions [62]. The ligands **2** and **3** failed to induce a structural transition from hybrid-type mixed parallel/antiparallel G-quadruplex to a parallel-stranded structure in the telomere G-quadruplex. A similar effect was seen in the case of the *BCL2* promoter G-quadruplex structure (Fig. 3C). It is interesting to note that the ligands **1**, **2**, **3**, **4** or **5** induced changes in the ellipticity of human *c-MYC, c-KIT1, c-KIT2* and *VEGF* promoter G-quadruplexes; however, the parallel-stranded topology was retained (Fig. 3B, 3D-3F). These results suggest that these ligands

preferentially bind to the parallel-stranded G-quadruplexes formed by G-rich promoter sequences derived from human *c-MYC*, *c-KIT1*, *c-KIT2* and *VEGF* oncogenes. Based on these observations, we propose that the benzimidazole-carbazole ligands induce and stabilize parallel-stranded G-quadruplex topologies. Moreover, the piperazine residues at the end of the benzimidazole scaffold (ligand **1**, **4**, and **5**) play an important role in the structural alteration of hybrid G-quadruplex structures into parallel ones. Interestingly, replacement of the piperazine residues with morpholine (ligand **2** and **3**) disable the molecules to bring about any such transformational changes.

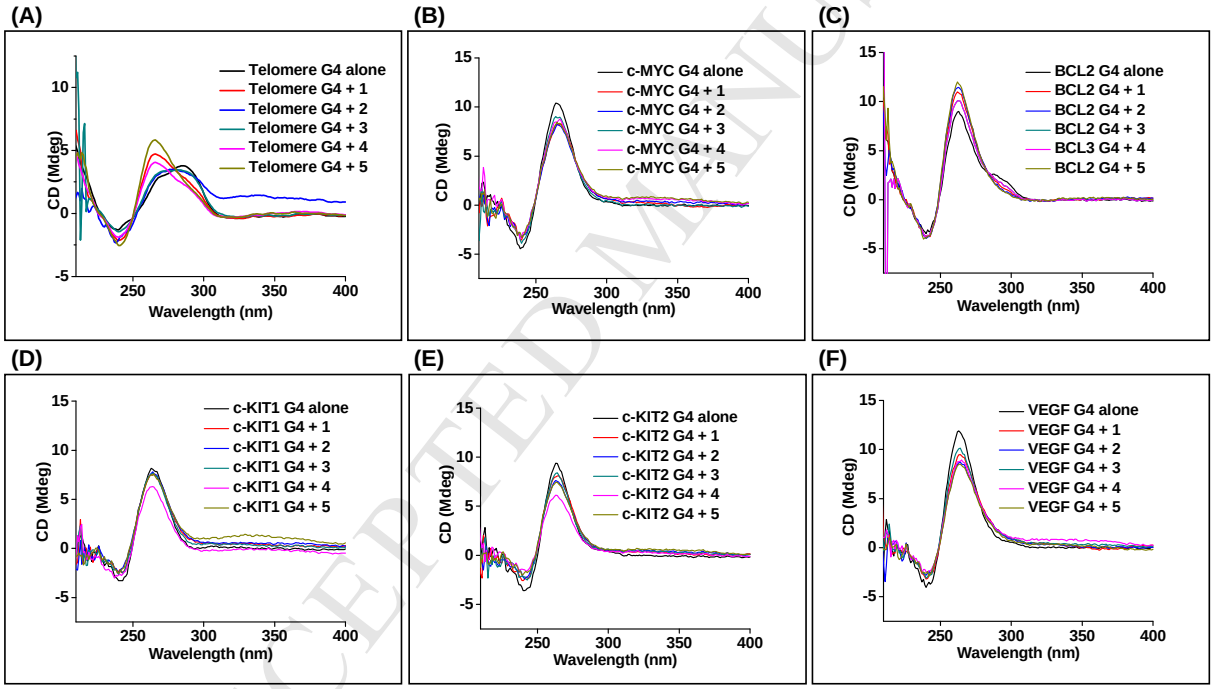

Figure. 3. The effect of benzimidazole-carbazole ligands on the conformation of different G-quadruplex substrates. The CD spectra were obtained from reaction mixtures containing 5 μM of the indicated G-quadruplex in 10 mM Tris-HCl buffer (pH 7.4) with 100 mM KCl, 0.1 mM EDTA in the presence or absence of different ligands. Inset: black, red, blue, dark cyan, pink and olive CD spectral tracings correspond to G-quadruplex in the absence or presence of ligands **1, 2,**

3, 4 and **5**, respectively. Panels A, B, C, D, E, and F correspond to telomeric, c-*MYC*, *BCL2*, *c-KIT1*, *c-KIT2* and *VEGF* G4 DNA substrates respectively.

2.4. Fluorescent intercalator displacement assay

The fluorescent intercalator displacement (FID) assay has been previously used to determine the specificity and affinity of putative G4 DNA ligands [1-2,6-7]. Thiazole orange (TO), a fluorescent DNA-binding ligand, binds to G-quadruplexes with high affinity; it does so in a manner consistent with binding at a single site, leading to a 500 to 3000-fold increase in fluorescence emission [65]. The enhancement in fluorescence emission appears to depend on the topology of G-quadruplex that adopted by a given G-rich sequence. The affinity of a given ligand for G-quadruplex is expressed in terms of DC_{50} values, which represents the concentration of the ligand required to reduce the fluorescence intensity by 50%. A low DC_{50} value suggests high binding affinity and vice versa.

We have previously shown that benzimidazole-carbazole conjugates display lower DC_{50} values for telomeric G-quadruplexes compared to duplex DNA, suggesting higher affinity of the ligands towards G-quadruplex structures [42]. These findings were further validated by determining the concentrations of ligands **1**-**5** required to reduce the fluorescence intensity of oncogene promoter (*c-MYC*, *c-KIT1*, *c-KIT2*, *VEGF*, and *BCL2*) G-quadruplexes (Fig. 4; supplementary Fig. S5-S7 and Table 2). The ligand **1** showed higher affinity towards *c-MYC*, *c-KIT1*, *c-KIT2*, and *VEGF* with DC_{50} values of 1.63 μM, 1.62 μM, 1.36 μM and 1.42 μM respectively (Table 2). However, a higher concentration of ligand **1** was required to displace 50% of TO from telomeric and *BCL2* G-quadruplexes. The DC_{50} values for ligand **1** were 2.79 μM and 2.86 μM in the case of telomeric and *BCL2* G-quadruplexes, respectively. To assert the

generality of the principle, DC_{50} values were determined for ligands **2**, **4** and **5**. The ligands **2**, **4** and **5** displayed lower DC_{50} values for *c-MYC, c-KIT1, c-KIT2* and *VEGF* over telomeric and *BCL2* G-quadruplexes (Table 2). Notably, ligands **2**, **4** and **5** displayed higher efficiency compared to ligand **1**, indicating higher affinity for G4 DNA. This higher affinity may be due to the presence of the extra protonated side chain coupled to the carbazole *N*-centre. However, higher DC_{50} values for ligand **3** indicates that the existence of an additional protonatable morpholine moiety along the carbazole *N*-side chain energetically disfavors the G-quadruplex binding activity. Importantly, all the ligands (**1**–**5**) displayed increased binding affinity towards parallel G-quadruplex structures (*c-MYC*, *c-KIT1*, *c-KIT2*, and *VEGF*) over hybrid-type structures (telomere and *BCL2*). The standard G-quadruplex DNA binding molecule TMPyP4 showed higher affinity towards all the G-quadruplex DNA than the carbazole-benzimidazole ligands (supplementary Fig. S8 and Table 2). It is important to note that, unlike carbazole-benzimidazole ligands, TMPyP4 does not show any preference among different G-quadruplex DNA topologies. Moreover, all the carbazole-benzimidazole ligands showed much higher selectivity toward *ds*-DNA over G-quadruplex DNA than TMPyP4 (Table 2).

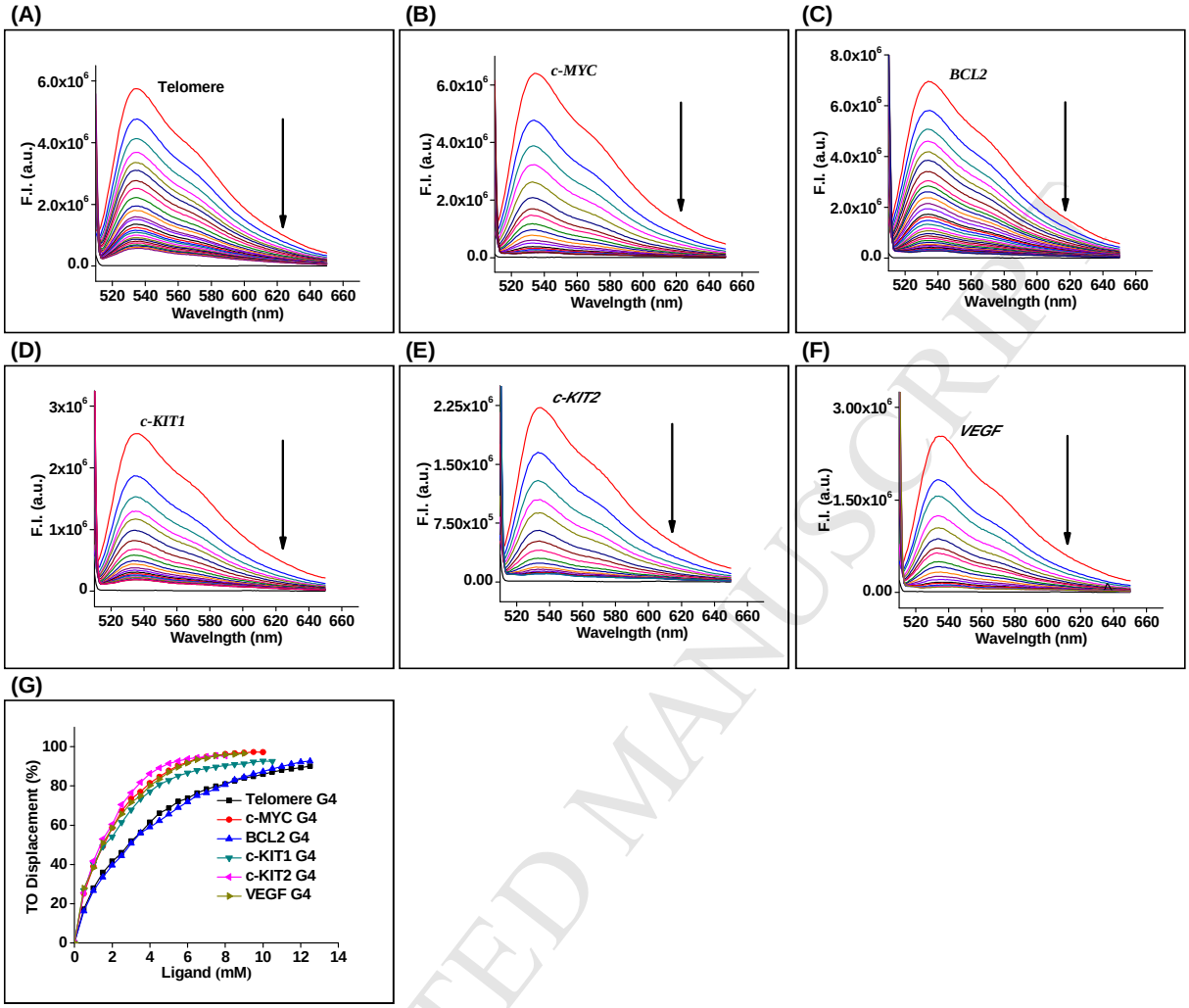

Fig. 4. Thiazole orange (TO) displacement by ligand **1** from telomeric, *c-MYC*, *BCL2*, *c-KIT1*, *c-KIT2* or *VEGF* G-quadruplex-TO adduct. The fluorescence spectra of TO/G-quadruplex was obtained in a buffer containing 10 mM Tris-HCl (pH 7.4), 100 mM KCl, and 0.1 mM EDTA in the presence of increasing concentrations of ligand **1**. The fluorescence spectral tracings were recorded at each time point after the addition of an aliquot of a ligand (0.15 μM). Panels A, B, C, D, E, and F correspond to telomeric, *c-MYC*, *BCL2*, *c-KIT1*, *c-KIT2* and *VEGF* G4 DNA substrates respectively. Panel G shows relative TO displacement for telomeric, *c-MYC*, *BCL2*, *c-*

KIT1, *c-KIT2* and *VEGF* G-quadruplex substrates as a function of increasing concentration of the specified ligand (as indicated in each panel).

Table 2. DC_{50} values (ligand concentrations for the displacement of 50% of the TO from G4 DNA-TO complex) for the different G-quadruplexes as determined from fluorescence intercalator displacement assays[a].

[a]The results are the average of two independent experiments and estimated error values are within ± 5% of each other.

2.5. Thermal stability of telomere and oncogene promoter G-quadruplexes

The data from fluorescence titrations and the FID assay suggest that ligands **1**-**5** bind efficiently to both telomeric and oncogene promoter (*c-MYC*, *c-KIT1*, *c-KIT2* and *VEGF*) G-quadruplexes. To further validate these observations, we examined the thermal stability (ΔT_m) of telomeric and oncogene promoter (*c-MYC*, *c-KIT1*, *c-KIT2* and *VEGF*) G-quadruplexes as a function of ligands **1-5** using CD spectroscopy. Toward this end, the samples (in 10 mM Tris-HCl buffer, pH 7.4) containing 5 µM G-quadruplex DNA, 25 mM KCl and 0.1 mM EDTA and different ligands were heated followed by slow cooling to room temperature. The variable

temperature CD spectra were recorded on a Jasco J-810 spectropolarimeter. Since benzimidazole–carbazole conjugates induce a parallel topology in telomeric G4 DNA, melting studies were carried out at 264 nm.

The Fig. 5A shows thermal melting profiles for telomeric G4 DNA in the absence or presence of ligands **1**-**5**. In the absence of any ligand, the telomeric G-quadruplex showed a T_m of 55.3 °C. In the presence of ligands **1**-**5**, the T_m increased up to 21.2 °C. As shown in Table 3, the ΔT_m values are quite high for ligands **2**, **4** and **5** at 16.8 °C, 21.1 °C and 21.2 °C respectively. The ΔT_m values are lower for ligands **1** and **3** at 9.7 °C and 7.1 °C respectively (Table 3). Thus, these experiments reveal that ligands **1**-**5** confer thermal stability on the telomeric G-quadruplex structure.

Next, we investigated the effect of ligands on stabilization of oncogene promoter G-quadruplexes. As these promoter G-quadruplexes are known to adopt a parallel topology in the presence of K^+ ion, the melting studies were followed at 262 nm. The CD melting measurements showed significant thermal stabilization of promoter G-quadruplex DNAs in the presence of each ligand (Fig. 5B-5F). The thermal stability provided by ligands **1**-**5** to promoter G-quadruplexes followed the order *c-KIT1* ≈ *c-KIT2* > *VEGF* > *c-MYC* ≈ *BCL2*. The ΔT_m values for various G-quadruplexes are in the range 6.5–17 °C for ligand **1**; 5.6-16.8 °C for ligand **2**; 3.3–7.5 °C for ligand **3**; 8.9–25.9 °C for ligand **4** and 7.4–24.7°C for ligand **5** (Table 3). The ligands **1**, **2**, and **3** provided slightly less thermal stabilization compared to ligands **4** and **5**. However, there was no clear order of magnitude in the stabilization provided by various ligands to different G-quadruplexes. The ligands **4** and **5**, having three protonatable side chains with either piperazine or dimethylamine residues, showed enhanced stabilization compared to ligand **1** (having only two side chains). The ligand **2,** with two morpholine residues, exhibited moderate stabilization

while compound **3** (containing an additional morpholine moiety that, however, blocks the piperazine side-chain) exhibited a much weaker stabilizing ability and selectivity for all the investigated quadruplexes. The standard G-quadruplex DNA binder TMPyP4 conferred much lower thermal stability to G-quadruplex DNA than ligand **4** or **5**.

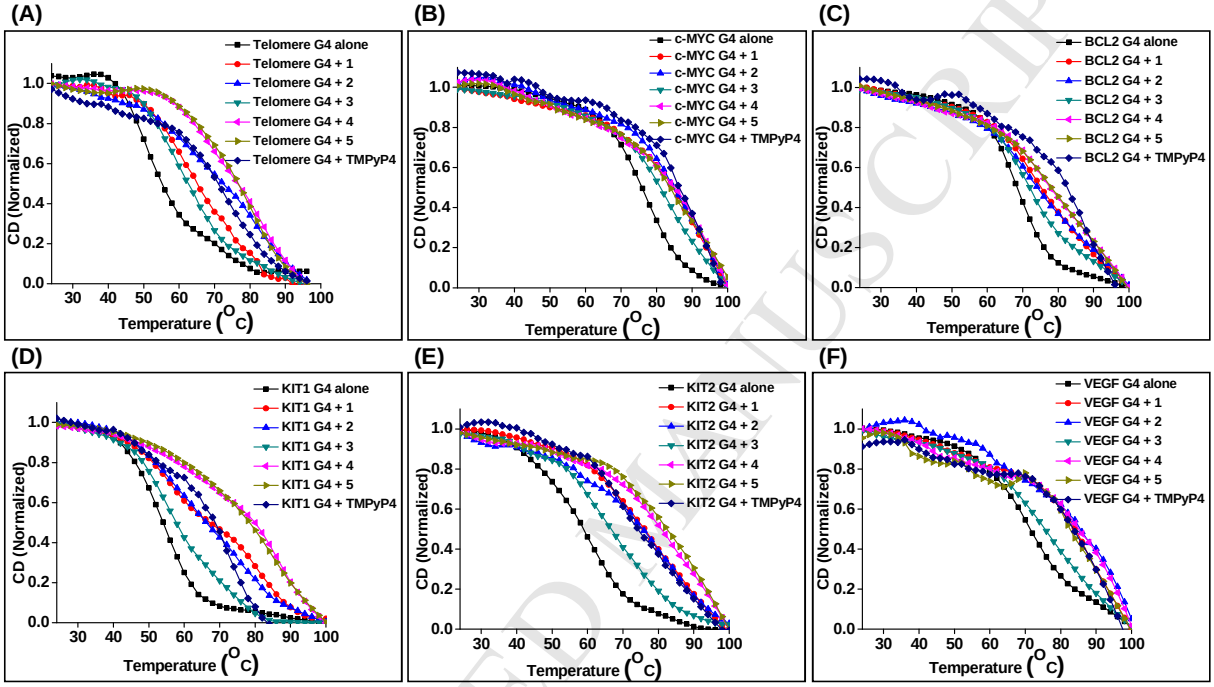

Fig. 5. Benzimidazole–carbazole ligands stabilize telomeric, *c-MYC*, *BCL2*, *c-KIT1*, *c-KIT2* and *VEGF* G-quadruplex structures. Thermal denaturation studies of G-quadruplex in the absence or presence of ligands **1, 2, 3, 4**, **5** or **TMPyP4.** Black, red, blue, dark cyan, pink, olive and dark blue spectral tracings correspond to the thermal denaturation profiles in the absence and presence of ligand **1, 2, 3, 4**, **5** and **TMPyP4** respectively. Panels A, B, C, D, E, and F correspond to telomeric, *c-MYC*, *BCL2*, *c-KIT1*, *c-KIT2* and *VEGF* G-quadruplex substrates, respectively.

Table 3. Thermal stability of various G-quadruplex DNA structures with different benzimidazole–carbazole conjugates measured by CD melting studies[a].

[a]ΔT_m values were obtained from the differences in the melting temperatures of the ligand bound and G4 DNA alone in 10 mM Tris−HCl buffer (pH 7.4) containing 25 mM KCl and 0.1 mM EDTA. The results are the average of two independent experiments and are within ± 0.5 °C of each other.

Our previous studies with telomeric G-quadruplex showed relatively weaker stabilization by ligands in the presence of NaCl compared with G-quadruplex stabilized by KCl [42, 43]. In the presence of Na^+ ion, the ligands failed to bring about a conformational change in telomeric G4 DNA from antiparallel basket to parallel type; however, in the case of K^+ ion, the ligands bring about a conformational change and they favor parallel conformation. Thus, the higher denaturation temperatures in the presence of K^+ ion are most likely due to the topological transformation from hybrid to a more stable parallel structure. This suggests that the parallel form of G-quadruplexes meets the structural requirements for maximum non-covalent interactions with the ligands. Collectively, the results from CD melting studies suggest that ligands **1**-**5** preferentially stabilize parallel the G-quadruplex conformation.

2.6. Polymerase stop assay

Having established that ligands **1-5** interact with and stabilize promoter G-quadruplex structures, we asked whether such stabilized G-quadruplexes present obstacles to DNA synthesis by DNA polymerases. For this purpose, a 77-mer *c-MYC* G-quadruplex forming sequence was annealed to ^{32}P-labeled primers through heating followed by slow cooling in 10 mM Tris-HCl buffer (pH 7.4) containing 5 mM KCl. The concentration of the primer used for annealing was 1.5-fold higher than the template and targeted towards a complementary region at the 3′ end of the template. The primer extension reaction was initiated by the addition of *Taq* DNA polymerase. The reaction was performed at 48 °C for 30 min. As expected, the reaction performed in the absence of any added ligand generated a full-length product (Fig. 6A, lane 2).

In theory, if the ligand stabilizes a G-quadruplex structure in the *c-MYC* template, the primer extension by *Taq* DNA polymerase would pause at the G-quadruplex-forming (pause) site. On adding increasing concentrations of ligand **5**, enhanced pausing was observed at the site coinciding with the formation of G-quadruplex in the 77-mer *c-MYC* G-rich promoter sequence (Fig. 6A, lanes 3 to 6). These results suggest that ligand **5** enhances Taq DNA polymerase pausing by stabilizing the G-quadruplex structure. At high concentrations of ligand **5**, there was increased premature termination resulting in complete inhibition of the formation of full-length products.

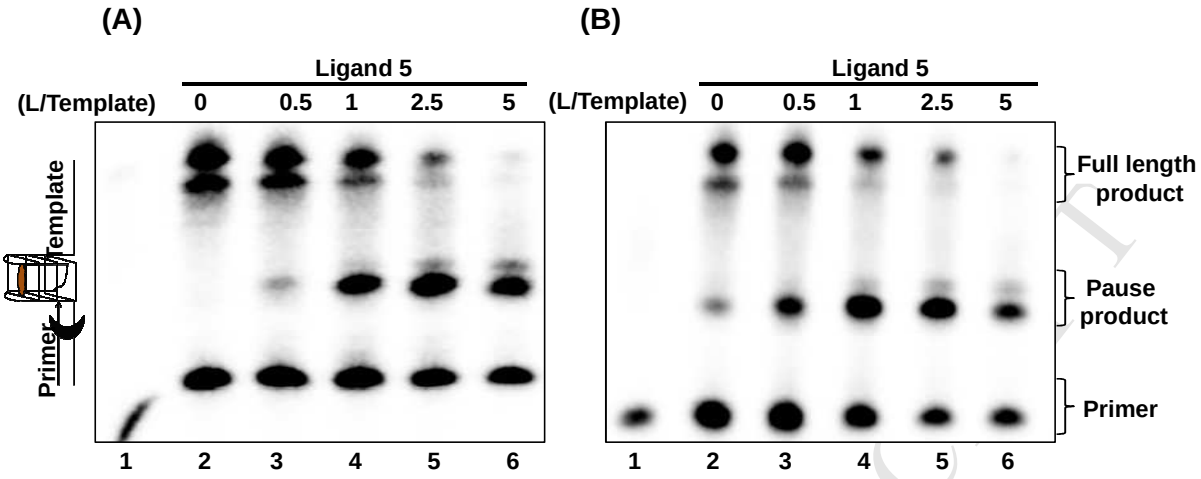

Figure. 6. *Taq* DNA polymerase stop assay performed on the *c-MYC* DNA template sequence in the presence of increasing concentrations ligand **5** and **1**. The position of primer, full-length product and the pause product is indicated on the right-hand side. (A) Primer extension reaction in the presence of ligand **5** at 48 °C. (B) Primer extension reaction in the presence of ligand **1** at 40 °C.

To further substantiate these findings, *Taq* DNA polymerase primer extension reactions were carried out using ligand **1** at 40 °C. As shown in Fig. 6B (lane 1), in the absence of ligand **1**, a small amount of ligand-independent DNA synthesis arrest was seen at the guanine tract. In contrast, ligand **1** generated the same premature chain termination products as ligand **5**, confirming that these ligands are responsible for blocking DNA synthesis. Furthermore, the extent of premature chain termination observed was directly proportional to the concentration of ligand added to the reaction (Fig. 6B, lanes 3-6). The pattern and extent of ligand-dependent arrest of DNA synthesis is consistent with the notion of stabilization of G-quadruplex DNAs formed by oncogene promoter G-rich sequences.

2.7. Computational studies

To investigate the most probable modes of binding of these ligands to various G-quadruplex structures at the telomeric and oncogene promoter regions, we performed docking studies using the AutoDock 4.0 software [64]. In addition, the extent of binding of these ligands to various G4 DNAs was determined, thus substantiating the biophysical results described above. For this purpose, two representative benzimidazole–carbazole conjugates were taken for docking studies namely: ligand **1** and **2**. Initially, the energy optimization of ligands **1** and **2** was performed and the most stable energy state structures were obtained. These were then docked with the structures of human *c-KIT* (2O3M), *c-KIT2* (2KQH), *VEGF* (2M27), H_{Telo} (1KF1), *c-MYC* (1XAV), and *BCL2* (2F8U) G-quadruplexes (Fig. 7). Both the ligands were found to interact with different G-quadruplexes through efficient stacking and/or H-bond formation. Primarily the central benzimidazole–carbazole pharmacophore interacted with the planar G-tetrad; the side chains were found to interact with the negatively charged phosphate backbone in the groove and loop region. Taken together, these results corroborate the spectroscopic analysis and DNA synthesis arrest studies showing that ligands **1** and **2** efficiently interact with the G-quadruplex structures formed by both telomere and oncogene promoter G-rich sequences.

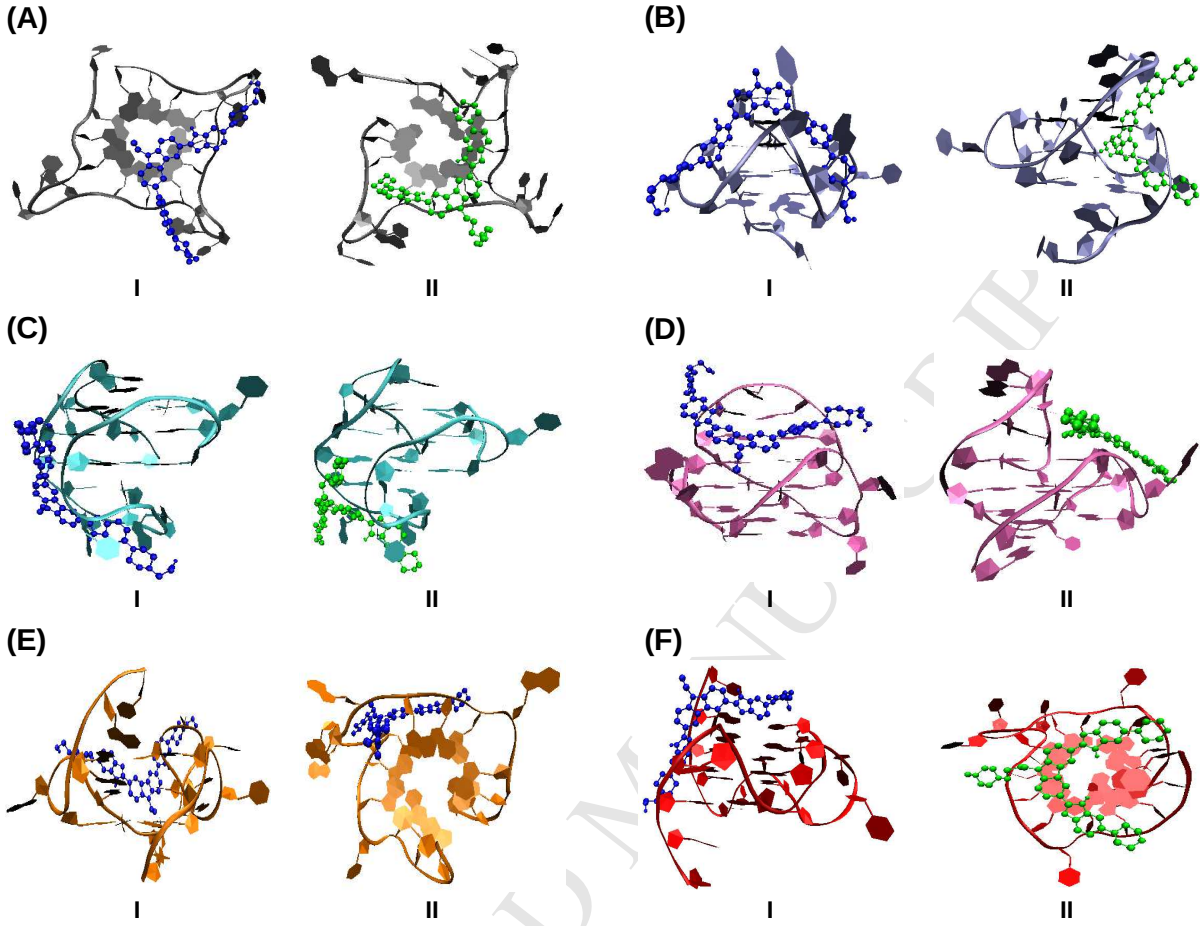

Figure. 7. The docked models of ligands **1** and **2** with (A) telomeric, (B) *c-MYC*, (C) *BCL2*, (D) *c-KIT1*, (E) *c-KIT2* and (F) *VEGF* G-quadruplex structures. PDB code of the telomeric, *c-MYC*, *BCL2*, *c-KIT1*, *c-KIT2* and *VEGF* G-quadruplex structure used for the docking are 1KF1, 1XAV, 2F8U, 2O3M, 2KQH, and 2M27 respectively. Panel I represent docking with ligand **1** and subpanel II with ligand **2**.

2.8. Benzimidazole–carbazole ligands inhibit telomerase activity and oncogene expression, which in turn shows cancer cell specific cytotoxicity

The foregoing studies demonstrate that telomeric and oncogene promoter G-quadruplex structures can be stabilized by benzimidazole-carbazole ligands. Next, we sought to investigate their ability to inhibit telomerase activity; to bind and repress the transcription of target oncogene promoters. To this end, the effect of ligand **5** on telomerase activity was tested using a modified telomeric repeat amplification assay (TRAP-LIG) [65]. Here, ligand **5** was used in the concentration range of 0.01 to 2 μM. As shown in Fig. 8A, it inhibited telomerase activity in a dose-dependent manner, and this was correlated with the decreased intensity and number of telomeric bands with an IC_{50} value of 0.3 μM. We wondered whether ligand **5** can suppress the expression of *c-MYC* and *VEGF* gene products in cell models. Accordingly, we analyzed their transcriptional response to ligand **5** in MCF-7 and HeLa cells using qRT-PCR assay. The expression of the housekeeping gene GAPDH served as a control. We found a dose-dependent decrease in *c-MYC* and *VEGF* transcript levels with no alteration in *GAPDH* transcription. The HeLa cells showed 49% and 71% decrease in *c-MYC* transcription upon treatment with 5 μM and 10 μM ligand **5**, respectively; however, no corresponding reduction was seen in cells treated with DMSO (Fig. 8B). Similarly, the VEGF transcript levels were reduced by 44% and 68% upon treatment with 5 μM and 10 μM of ligand **5** respectively.

Next, we evaluated whether these ligands exhibit anti-proliferative effect against various cancer cell lines. The cytotoxic efficacy of ligand **5** against human breast cancer cells (MCF-7) and human cervical cancer (HeLa) cells was carried out using MTT assay. The results showed that ligand **5** significantly inhibited the proliferation of cancer cell lines in a concentration-dependent manner with IC_{50} values of 11.42 μM and 8.29 μM respectively (Fig. 8C). Thus, these

results support the idea that benzimidazole-carbazole ligands could potentially be used for suppression of oncogene expression in cancer cells, and as suitable candidates in cancer chemotherapy.

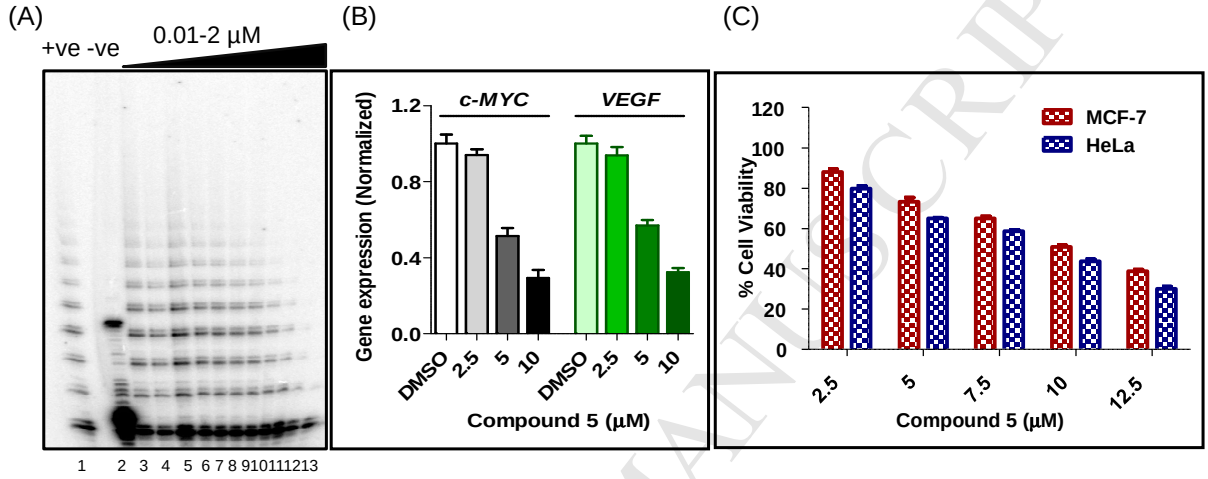

Figure 8. Benzimidazole–carbazole ligand **5** inhibits telomerase activity, represses oncogene expression and displays cancer cell specific cytotoxicity. (A) Ligand **5** inhibits telomerase activity in a dose-dependent manner. Telomerase inhibition of ligand **5** was evaluated by TRAP–LIG assay. Lane 1, positive control; 2, negative control. Lanes 3-13, incubated with increasing concentrations of ligand **5** (0.01, 0.02, 0.04, 0.08, 0.1, 0.3, 0.6, 0.9, 1.2, 1.5, 2 µM respectively). (B) Ligand **5** suppresses *c-MYC* and *VEGF* transcription in HeLa cells. The HeLa cells were treated with increasing concentrations of ligand **5** for 24 h and then the transcript levels of *c-MYC* and *VEGF* were measured. The histograms show relative fold change in the *c-MYC* and *VEGF* transcript levels upon ligand treatment. *GAPDH* was used as an internal control for normalization. (C) Ligand **5** decreases cell viability and induces cell death. Cytotoxic effect of ligand **5** in MCF-7 and HeLa cells was evaluated by the MTT assay. The error bars represent the mean ± SD of three independent experiments performed in triplicate

3. Conclusions

The biological significance of G-quadruplexes has been well-recognized and they have emerged as attractive candidates for cancer therapy. The interest in telomere-specific therapeutic compounds continues, in parallel, there is growing interest in oncogene promoter G-quadruplexes as potential therapeutic targets to design a new effective anticancer drug. In contrast to the telomeric G-quadruplex forming sequence, the G-quadruplex-forming sequences in promoter regions are diverse and can fold into multiple G-quadruplex conformations. Thus, the discovery and development of small molecules that can interact with genomic G-quadruplex DNA structures may provide necessary opportunities for targeting promoter sequences and downstream events. A ligand that stabilizes one structure may interact differently with others. Therefore, it is necessary to profile the interaction of ligands with different G-quadruplexes to determine their biological activity as G-quadruplex stabilizing compounds.

Our previous studies have demonstrated that benzimidazole-carbazole ligands preferentially bind to and stabilize telomeric G-quadruplexes over double-stranded DNA and, consequently, inhibit telomerase activity [42]. Additionally, these ligands exhibit selectivity towards parallel G-quadruplex structures. In the current study, benzimidazole-carbazole ligands were found to bind and stabilize human *c-MYC*, *c-KIT1*, *c-KIT2*, *VEGF* and *BCL2* promoter G-quadruplex structures *in vitro*. The spectroscopic experiments suggest that benzimidazole-carbazole ligands induce topological changes from hybrid to stable parallel G-quadruplex DNAs. Consistent with the experimental data on thermal stability of G-quadruplexes and FID assays, these ligands displayed higher affinity to oncogene promoter G-quadruplexes. Furthermore, studies with ligands **2**, **4** and **5** indicate that these are strong oncogene promoter G-quadruplex binding

ligands compared to ligands **1** and **3**. Structural modifications among ligands **1**–**5** strongly suggest that the hydroxyethyl substituted bis-benzimidazole residues are responsible for topological transformation of the G-quadruplex DNA structure. The additional protonatable residue at the carbazole *N*-centre (ligand **2**, **4**, and **5**) enhances G-quadruplex DNA affinity without altering the specificity toward parallel topological structure. Notably, the stabilization of promoter G-quadruplexes by benzimidazole–carbazole ligands stall DNA replication and inhibit oncogene expression *in vivo*. We close with a point emphasizing the notion that the transcriptional activation of oncogenes in cancer cells can be suppressed through the stabilization of G-quadruplexes by benzimidazole–carbazole ligands.

4. Experimental section

4.1 Synthesis of benzimidazole–carbazole ligands

We designed and synthesized ligand **1**, **3** and **5** (scheme 1-3) as previously described [42]. All starting materials were from the commercial sources and used without further purification. All solvents were from Merck, and they were distilled and/or dried prior to use whenever necessary. All ligands were found to be at least >95% pure by elemental analysis.

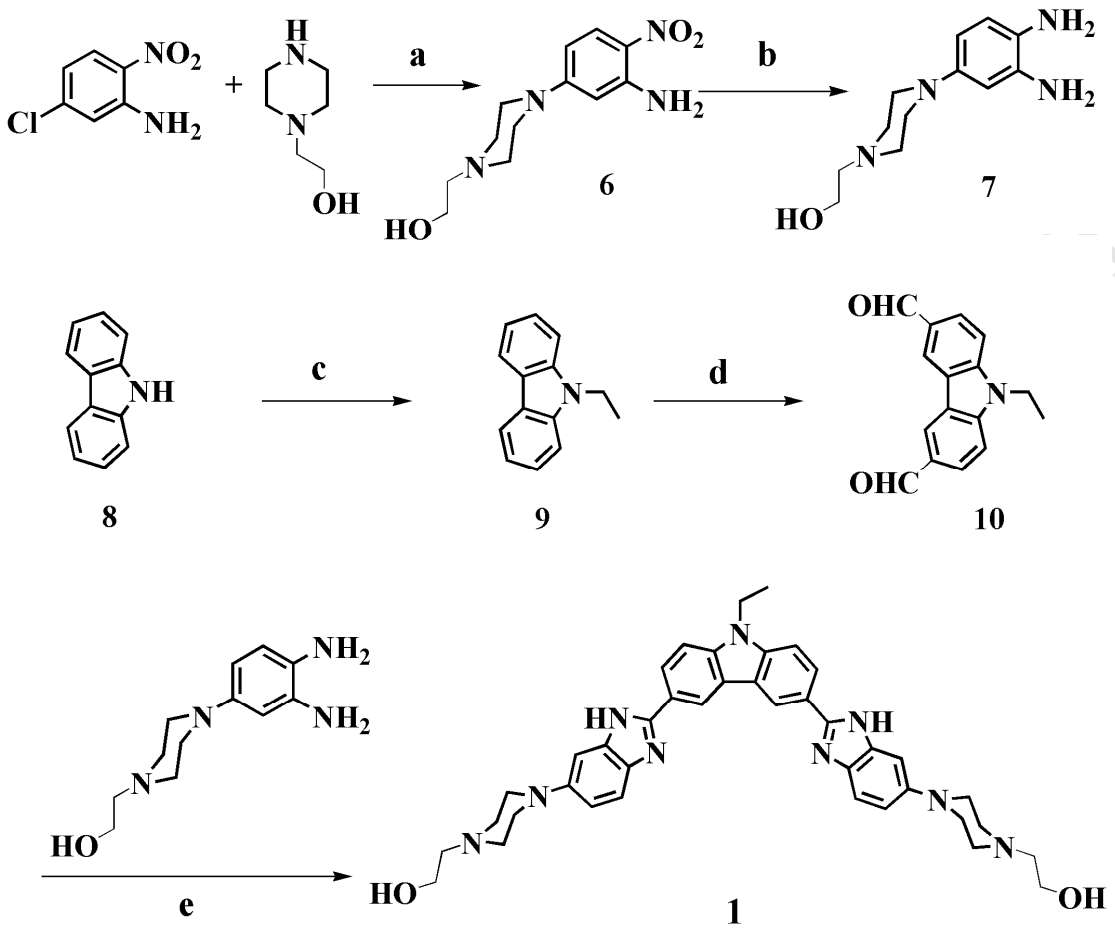

Scheme 1. *Reagents, conditions and yields*: a) dry DMF, K_2CO_3, N_2-atomosphere, 110 °C, 12 h, 95%, b) H_2/Pd-C, rt, 12 h, 100%, c) NaH, ethylbromide, TBAI, DMF, rt, 12 h, 80%, d) $POCl_3$, DMF, $ZnCl_2$, 100 °C, 24 h, 75%, (e) Compound **7**, $Na_2S_2O_5$, ethanol, 80 °C, 24 h, 60%.

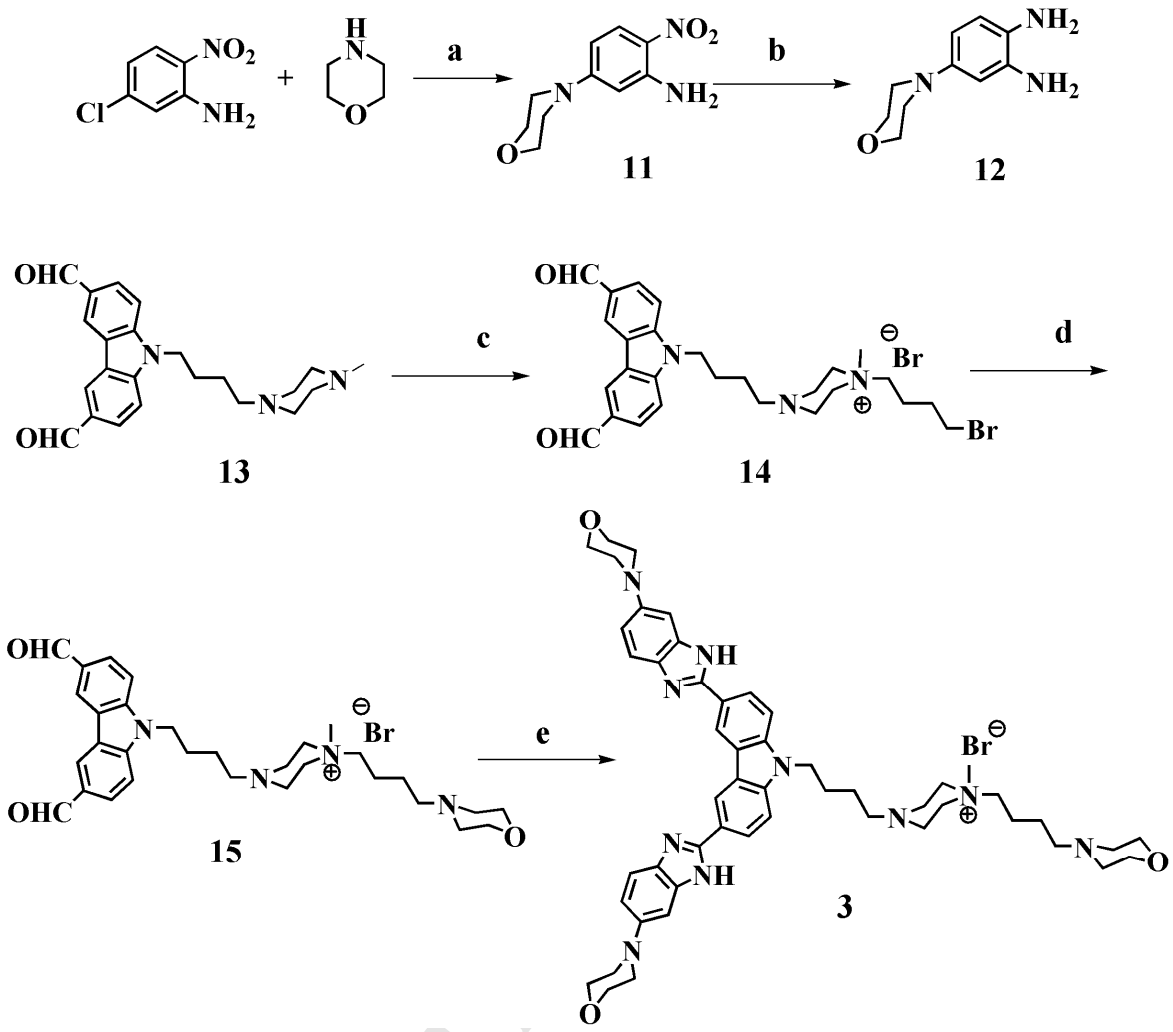

Scheme 2. *Reagents, conditions and yields***:** a) dry DMF, K_2CO_3, N_2-atm. 110 °C, 12 h, 95%, b) H_2/Pd-C, room temperature, 12 h, 100%, c) 1, 4-Dibromobutane, acetonitrile, 50 °C, 6 h, 90%; d) Morpholine, room temperature, 12 h, 98%, e) (**12**), $Na_2S_2O_5$, EtOH, 80 °C, 12 h, 85%.

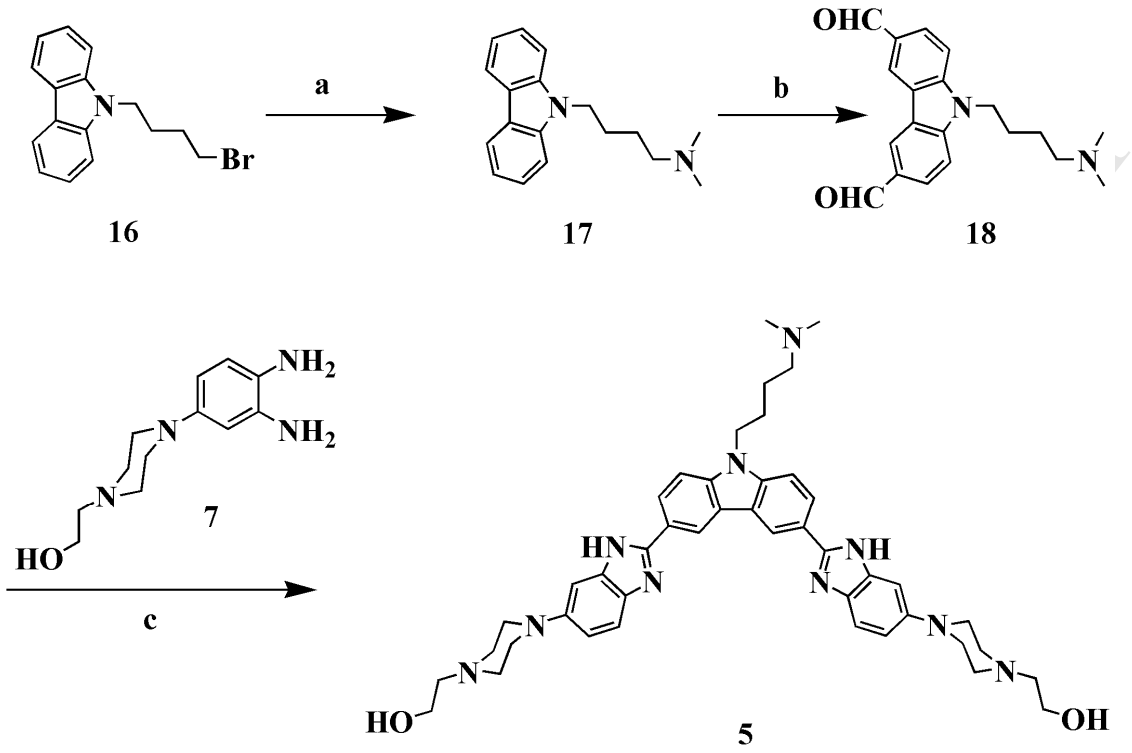

Scheme 3. *Reagents, conditions and yields***:** a) 1,4-dibromobutane, TBAI, 50% NaOH, room temperature, 12 h, 72%; b) $NHMe_2$(g), acetonitrile, 80 °C, 6 h, 90%; c) $ZnCl_2$, $POCl_3$/DMF, 0 °C → 100 °C, 24 h, 75%; d) compound **7**, $Na_2S_2O_5$, EtOH, 80 °C, 24 h, 70%.

2-[4-(3-Amino-4-nitro-phenyl)-piperazin-1-yl]-ethanol (**6**). 5-Chloro-2-nitroaniline (2 g, 11.6 mmol) was taken in dry DMF (5 ml) and 2-piperazin-1-yl-ethanol (3g, 23.08 mmol) and K_2CO_3 (4.8 g, 34.6 mmol) were added to the solution. This mixture was then heated at 110 °C under N_2 atmosphere for 12 h until the disappearance of 5-chloro-2-nitroaniline. The crude compound was suspended in water and the product was extracted with ethyl acetate. The organic layer was washed twice with water, dried over anhydrous Na_2SO_4 and

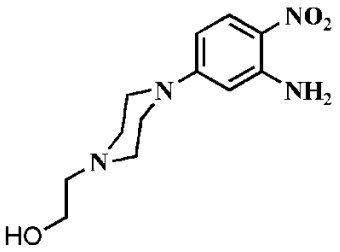

concentrated. This resulted in a pure product as confirmed by TLC (1% MeOH/$CHCl_3$ on pre-coated silica gel) and was isolated as a bright yellow solid (2.93 g, 95% yield). ^{1}H NMR (300 MHz, $CDCl_3$) δ ppm 2.59-2.65 (m, 6H), 3.4 (t, *J* = 4.8, 4H), 3.7 (t, *J* = 4.8, 2H), 5.95 (d, *J* = 2.7, 1H), 6.1 (bs, 2H, NH_2), 6.29 (dd, *J* = 9.3, *J* = 2.7, 1H), 8.02 (d, *J* = 9.3, 1H); HRMS: *m/z* = 267.1457 $[M+H]^+$, Calcd. = 267.1457 $[M+H]^+$; mp 163 °C.

2-(4-(3, 4-Diaminophenyl)piperazine-1-yl)ethanol (7). Compound **5a** (206 mg) was

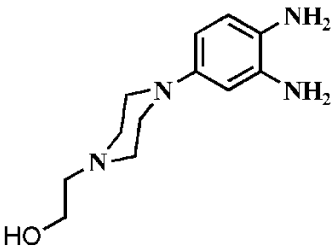

synthesized along with 100 mg of Pd/C (10%) in ethanol and stirred under a pressure of H_2 (1 atm.) for 12 h. The reaction mixture was passed through a celite bed under nitrogen flow and used for the next reaction without any further purification as the diamine product was found to readily undergo aerial oxidation.

9-ethyl-9H-carbazole (9). 2 g (12 mmol) of Carbazole (**8**) was dissolved in 20 ml of DMF and

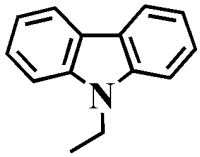

to that 115 (60 mmol) of NaH, 3.9 (36 mmol) of bromoethane and 440 mg (10%) were added and stirred at room temperature for 12 h. The reaction mixture was then quenched by slowly adding water and then dried under reduced pressure and partitioned between water and chloroform. The organic layer was passed through the Na_2SO_4 bed and dried to get crude white powder. The pure product was purified by column chromatography and the pure product was isolated at 2-3% ethylacetate/hexane eluent with a yield of 1.8 g (80%). ^{1}H NMR (300 MHz, $CDCl_3$) δ ppm 8.09 (d, *J* = 7.4, 2H), 7.45 (d, *J* = 7.4, 2H), 7.38 (d, *J* = 7.4, 2H), 7.21 (d, *J* = 7.4, 2H), 4.31 (q, *J* = 7.4, 2H), 1.4 (t, *J* = 7.4, 3H); HRMS: m/z = 196.1129 $[M+H]^+$, Calcd. = 196.1126 $[M+H]^+$.

9-ethyl-9H-carbazole-3,6-dicarbaldehyde (10). Compound **9** (1 g, 4 mmol), 1.56 g (8 mmol) of

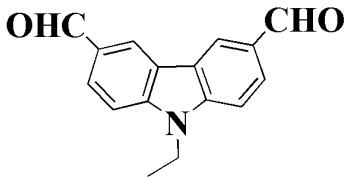

anhydrous $ZnCl_2$ were taken together in a round bottom flask (100 mL) along with 20 ml of dry DMF and heated at 100 °C for 15 min. This was followed by cooling to room temperature. To this solution, 3.7 ml (40 mmol) of $POCl_3$ was added drop-wise with cooling over ice-bath for 15 min followed by heating at 100 °C for 24 h. Then the reaction mixture was evaporated under vacuum to remove excess DMF and quenched by the addition of ice-cold water followed by neutralization with concentrated KOH solution. The mixture was finally extracted using ethyl acetate and the organic layer was passed through a bed of dry Na_2SO_4. The filtrate was collected and evaporated to get a brown gummy mass which was purified by silica gel column chromatography using chloroform/methanol as eluent. The final product was evident at 1% methanol/chloroform as an off-white solid, which was adjudged to be pure by TLC (1% MeOH/$CHCl_3$ on pre-coated silica gel) (1.5 g, 75%). ^{1}H NMR (300 MHz, $CDCl_3$) δ ppm 10.13 (s, 2H), 8.68 (s, 2H), 8.11 (d, *J* = 8.7, 2H), 7.55 (d, *J* = 8.4, 2H), 4.34 (q, *J* = 7.4, 2H), 1.47 (t, *J* = 7.4, 3H). HRMS: m/z = 252.1029 $[M+H]^+$, Calcd. = 252.1025 $[M+H]^+$.

Compound 1. 502 mg of compound **10** (2 mmol), 740 mg (4 mmol) of freshly prepared diamine

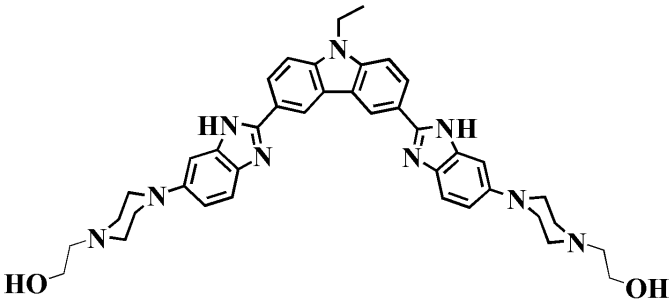

compound 7 were dissolved in 50 ml of ethanol and 461 mg of aqueous $Na_2S_2O_5$ was added and then heated at 100 °C for 24 h. Reaction mixture was then cooled and dried under reduced pressure and redissolved in methanol. The pure product was isolated by repeated precipitation from ethyl acetate with a yield of 819 mg (60%). ^{1}H NMR (400 MHz, d_6-DMSO) δ ppm 12.55 (broad, 2H), 9.06 (s, 2H), 8.3 (d, *J* = 8.8, 2H), 7.80 (d, *J* = 8.8, 2H), 7.46

(d, *J* = 8.4, 2H), 7.07 (s, 2H), 6.92 (d, *J* = 8.8, 2H), 4.81 (broad, 4H), 4.54 (s, 4H), 3.66 (t, *J* = 6, 4H), 2.93 (s, 12H), 2.77 (s, 6H), 1.36 (s, 3H). ^{13}C NMR (100 MHz, d_6-DMSO) δ ppm 152.72, 149.32, 142.32, 141.63, 124.43, 123.84, 122.65, 128.43, 112.21, 110.49, 60.12, 58.23, 53.45, 50.12, 13.56; HRMS: m/z = 684.3778 $[M+H]^+$, Calcd. = 684.3774 $[M+H]^+$. mp >300 °C; Anal. (calcd. for $C_{40}H_{45}N_9O_2$): C, 70.25; H, 6.63; N, 18.43; found: C, 70.75; H, 6.43; N, 18.22.

5-morpholino-2-nitrobenzenamine (11). A mixture of 5-chloro-2-nitrobenzenamine (1g, 1.8 mmol), morpholine (2 ml) and dry K_2CO_3 (1.2 g, 9 mmol) were taken along with 5 ml of dry DMF and heated at 110 °C under nitrogen atmosphere for 12 h. The reaction mixture was then dried under vacuum and 50 ml of cold water was added to it to form a yellow colored precipitate which was filtered off and washed several times with distilled water and then dried affording the yellow colored product which was adjudged to be pure by TLC (2% MeOH/$CHCl_3$ on pre-coated silica gel) (1.23g, 95%). ^{1}H NMR (400 MHz, d_6-DMSO) δ ppm 7.82 (d, *J* = 10, 1H), 7.28 (s, 2H), 6.39 (dd, *J* = 9.8, *J* = 2.8, 1H), 6.2 (d, *J* = 2.8, 1H), 3.70 (t, *J* = 4.8, H), 3.27 (t, *J* = 4.8, 4H); IR (KBr): 3448, 3335, 3179, 3088, 2973, 2928, 2872, 2846, 1618, 1234, 1123, 892 cm^{-1}; HRMS: m/z = 246.0858 $[M+Na]^+$, Calcd. = 246.0855 $[M+Na]^+$; mp 188 °C.

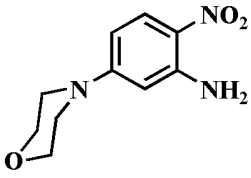

4-morpholinobenzene-1, 2-diamine (12). Compound **12** has been synthesized from compound **11** following a similar procedure as described for compound **7**.

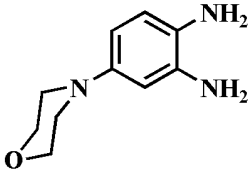

Compound 14. Compound **13** (1 g, 2.65 mmol) was taken with 20 mL of dry acetonitrile and to

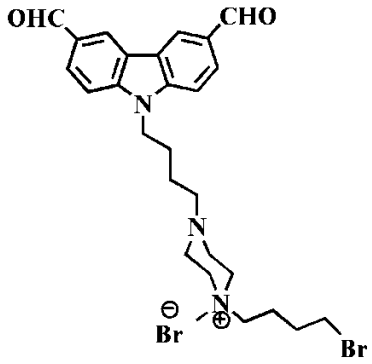

that 1,4-dibromobutane (2.3g, 10.6 mmol) was added and heated at 50 °C for 6 h. The volume was then reduced under vacuum and washed several times with petroleum ether followed by ethyl acetate to get a gummy yellowish product (1.42 g, 90%). ^{1}H NMR (400 MHz, CD_3OD) δ ppm 10.08 (s, 2H), 8.78 (s, 2H), 8.1 (dd, *J* = 8.8, 1.2, 2H), 7.78 (d, *J* = 8.4, 2H), 4.69 (m, 2H), 3.6-3.5 (m, 6H), 3.06 (s, 3H), 2.72 (s, 2H), 2.7-2.6 (m, 2H), 2.48 (t, *J* = 6.8, *J* = 6.8, 2H), 2.02-1.82 (m, 6H), 1.55 (m, 2H); HRMS: *m/z* = 512.1912 $[M\text{-}Br]^+$, Calcd. = 512.1913 $[M\text{-}Br]^+$.

Compound 15. The bromo-compound **14** (200 mg) has been taken with excess of morpholine

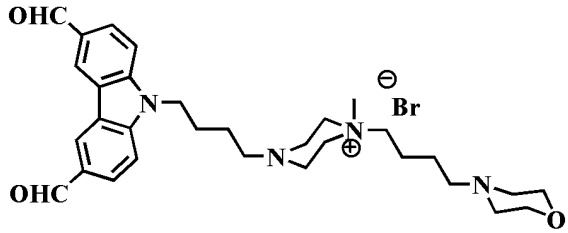

and stirred at room temperature for 12 h and then washed with ethyl acetate to get the pure product as gummy liquid (197 mg, 98%). ^{1}H NMR (400 MHz, d_6-DMSO) δ ppm 10.11 (s, 2H), 8.92 (d, *J* = 1.2, 2H), 8.09 (dd, *J* = 1.2, *J* = 8.8, 2H), 7.93 (d, *J* = 8.4, 2H), 4.57 (s, 2H), 3.9 (s, 4H), 3.78-3.76 (m, 4H), 3.72 (s, 2H), 3.65-3.61(m, 4H), 3.45 (t, *J* = 4.8, 2H), 3.1 (dd, J_1 = 4.8, J_2 = 5.8, 4H), 3.02 (s, 2H), 2.85 (t, *J* = 5.6, 2H), 2.71 (s, 2H), 2.60 (s, 2H), 2.42 (t, *J* = 6.8, 2H), 2.01 (s, 2H), 1.81 (s, 2H), 1.70 (s, 2H), 1.58 (s, 2H), 1.49 (s, 2H); IR (KBr): 1685 cm^{-1}; HRMS: m/z = 519.3336 $[M\text{-}Br]^+$, Calcd. = 519.3335 $[M\text{-}Br]^+$.

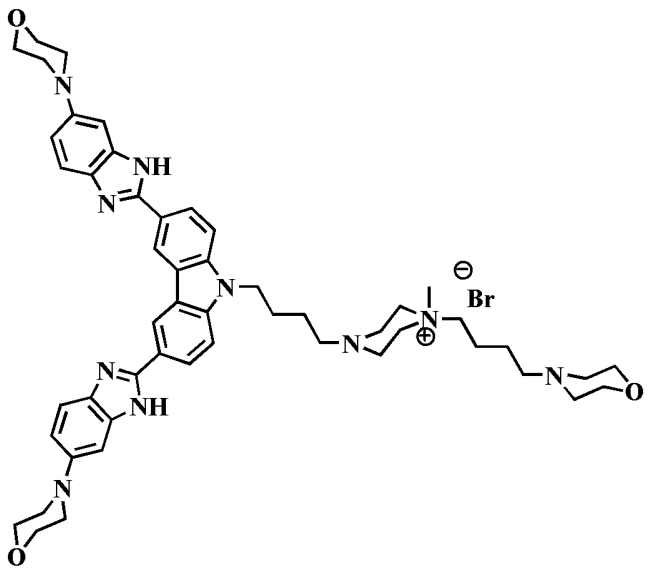

Compound 3. The compound **15** has been reacted with freshly prepared diaimine **12** following the similar procedure discussed earlier for compound **1** affording deep-

brown colored solid product with the yield of 85%. ^{1}H NMR (400 MHz, d_6-DMSO) δ ppm 9.09 (s, 2H), 8.30 (d, *J* = 8, 2H), 7.89 (d, *J* = 8.4, 2H), 7.54 (d, *J* = 8.8, 2H), 7.05 (d, *J* = 8.4, 2H), 4.54 (s, 2H), 3.9-3.72 (m, 16H), 3.62-3.56 (m, 3H), 3.46-3.39 (m, 9H), 3.04 (s, 4H), 2.85 (s, 2H), 2.76 (s, 2H), 2.67-2.63 (m, 2H), 1.86 (s, 2H), 1.7 (s, 4H), 1.53 (s, 2H); ^{13}C NMR (100 MHz, d_6-DMSO) δ ppm 150.59, 148.41, 141.71, 125.01, 122.35, 119.25, 115.11, 114.09, 110.56, 99.28, 66.21, 65.79, 63.34, 63.20, 61.47, 61.27, 59.19, 58.24, 57.36, 55.67, 5535, 51.21, 49.94, 47.86, 47.64, 47.43, 47.24, 45.52, 42.81, 42.59, 41.14, 26.20, 23.31, 20.74, 20.05, 18.52, 15.10; IR (KBr): 3445, 2952, 2922, 2853, 1642, 1449, 1260, 1110, 1044, 1021, 934, 899, 808 cm^{-1}; HRMS: m/z = 866.5319, Calcd. = 866.5319 $[M-Br]^+$; mp >300 °C; Anal. (calcd. for $C_{51}H_{65}BrN_{10}O_3$): C, 64.75; H, 6.93; N, 14.81; found: C, 64.88; H, 6.86; N, 14.73.

9-(4-Bromobutyl)-9H-carbazole (16). To a mixture of TBAI (277 mg, 0.75 mmol), carbazole (3

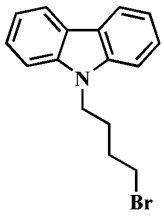

g, 18 mmol) and 11.67 g (54 mmol) of 1, 4-dibromobutane and an aqueous 50% NaOH (9 mL) were added at room temperature. The mixture was then stirred for 6 h and then poured into water (100 mL) and extracted with DCM. The organic layer was passed through a bed of dry Na_2SO_4 and evaporated to get a crude product which was purified by silica gel column chromatography with hexane/ethyl acetate mixture as eluent yielding a white solid (5.4 g, 90%). ^{1}H NMR (400 MHz, $CDCl_3$) δ ppm 8.1 (d, *J* = 7.6, 2H), 7.47 (m, 4H), 7.24 (dd, *J* = 4.5, 7.8, 2H), 4.36 (m, 2H), 3.38 (m, 2H), 2.07 (m, 2H), 1.91 (m, 2H); HRMS: m/z = 302.0545 $[M+H]^+$, Calcd. = 302.0544 $[M+H]^+$; mp 101 °C.

4-(9H-carbazol-9-yl)-N,N-dimethylbutan-1-amine (17). Compound **16** (900 mg, 2.98 mmol)

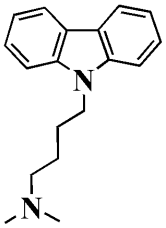

was dissolved in dry acetonitrile in a pressure tube and cooled down in ice. A dry dimethylamine was passed through the reaction mixture and stirred overnight at

80 °C. The excess dimethylamine was carefully removed and the reaction mixture was dried under reduced pressure. The crude product partitioned between water and chloroform. The organic layer was passed through a bed of dry Na_2SO_4. The filtrate was collected and evaporated to get the desired product which was adjudged to be pure by TLC (3% MeOH/$CHCl_3$ on pre-coated silica gel) (713 mg, 90%). ^{1}H NMR (400 MHz, $CDCl_3$) δ ppm 8.08 (d, *J* = 7.6, 2H), 7.45 (m, 4H), 7.24 (m, 2H), 4.39 (d, *J* = 5.1, 2H), 2.82 (m, 2H), 2.59 (s, 6H), 2.01-1.94 (m, 2H), 1.88-1.82 (m, 2H). HRMS: m/z = 267.1865 $[M+H]^+$, Calcd. = 267.1861 $[M+H]^+$.

9-(4-(dimethylamino)butyl)-9H-carbazole-3,6-dicarbaldehyde (18). Compound **17** (830 mg, 3.12 mmol), 850 mg (6.24 mmol) of anhydrous $ZnCl_2$ were taken together in a round bottom flask (100 ml) along with 6 ml of dry DMF and heated at 100 °C for 15 min. This was followed by cooling to room temperature. To this 2.9 ml (31.2 mmol) of $POCl_3$ was added drop-wise with cooling over ice-bath for 15 min followed by heating at 100 °C for 24 h. Then the reaction mixture was evaporated under vacuum to remove the excess DMF and quenched carefully by addition of ice-cold water followed by neutralization with concentrated KOH solution. The mixture was finally extracted using ethyl acetate and the organic layer was passed through a bed of dry Na_2SO_4. The filtrate was collected and evaporated to get a brown gummy mass which was purified by silica gel column chromatography using chloroform/methanol as eluent. The final product came at 3% methanol/chloroform as a brown solid which was adjudged to be pure by TLC (5% MeOH/$CHCl_3$ on pre-coated silica gel) (753 mg, 75%). ^{1}H NMR (400 MHz, $CDCl_3$) δ ppm 10.14 (s, 2H), 8.68 (s, 2H), 8.09 (dd, *J1* = 0.8, J2 = 8.4, 2H), 7.57 (d, 2H), 4.43 (t, *J* = 7.2, 2H), 2.29 (t, *J* = 7.2, 2H), 2.18 (s, 6H), 1.96 (t, *J* = 7.6, 2H), 1.56 (m, 2H). HRMS: m/z = 323.1763 $[M+H]^+$, Calcd. = 323.176 $[M+H]^+$.

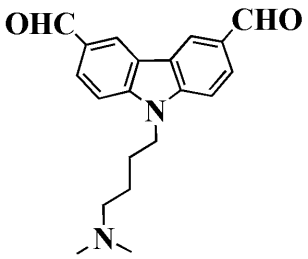

Compound 5. The dialdehyde compound **18** (200 mg, 0.62 mmol) was taken with freshly prepared diamine **7** (293 mg, 1.24 mmol) in 30 mL ethanol and to that 143 mg of aqueous $Na_2S_2O_5$ was added and refluxed for 12 h. The reaction mixture was then cooled and filtered and dried under reduced pressure to get the crude product. The mass was then dissolved in methanol and precipitated by addition of ethyl acetate. Repetitive precipitation yielded a light brown solid product (327 mg, 70%). ^{1}H NMR (400 MHz, d_6-DMSO) δ ppm 9.07 (s, 2H), 8.3 (d, *J* = 8.8, 2H), 7.79 (d, *J* = 8.8, 2H), 7.45 (d, *J* = 8.4, 2H), 7.02 (s, 2H), 6.92 (d, *J* = 8.8, 2H), 4.48 (s, 4H), 3.56 (t, *J* = 6, 4H), 3.16-3.12 (m, 8H), 2.62 (s, 8H), 2.48 (s, 6H), 2.3-2.22 (m, 4H), 1.8 (s, 2H), 1.57 (s, 2H); ^{13}C NMR (d_6-DMSO) δ ppm 153.27, 149.17, 142.23, 139.22, 135.41, 125.52, 124.11, 121.36, 120.21, 116.44, 115.81, 110.59, 101.58, 65.23, 60.36, 58.89, 54.78, 54.34, 44.25, 27.11, 24.52, 22.33, 15.18; HRMS: m/z = 755.4506 $[M+H]^+$, Calcd. = 755.4509 $[M+H]^+$; mp >300 °C; Anal. (calcd. for $C_{44}H_{54}N_{10}O_2$): C, 70.00; H, 7.21; N, 18.55; found: C, 70.8; H, 7.42; N, 18.31.

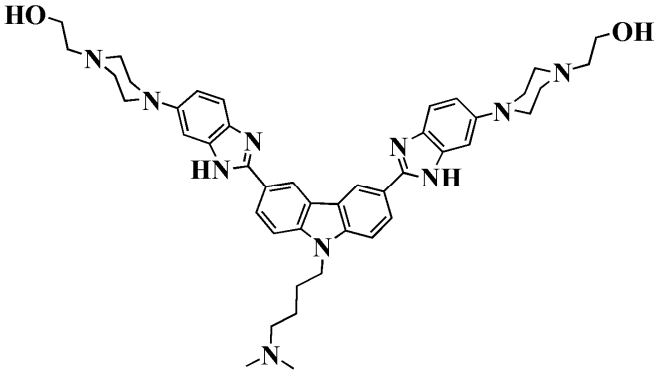

4.2 Oligonucleotides and reagents

The oligonucleotides used in this study were purchased from Sigma-Genosys Ltd. Oligonucleotide sequences used in this study are listed in Table 3. The oligonucleotides were suspended in TE buffer (10 mM Tris-HCl, 0.1 mM EDTA, pH 8.0) and stored at -20 °C. Molecular biology grade chemicals including polyethylene glycol 200 and thiazole orange (TO) were purchased from Sigma-Aldrich (Bangalore). All other reagents and biochemicals were

obtained from Sigma-Aldrich or from other commercial sources and used without further purification. The buffer solutions were prepared using Milli-Q water. Benzimidazole–carbazole conjugates used in the study were >95% pure. The ligand solutions were prepared in Milli-Q water/molecular biological grade DMSO and diluted in the corresponding buffer.

4.3 *G4 DNA sample preparation*

The G-rich oligonucleotides were prepared by dissolving in 10 mM Tris-HCl buffer (pH 7.5), 0.1 mM EDTA and indicated concentrations of KCl. They were folded into the G-quadruplex structure by heating at 95 °C for 5 min followed by slow cooling to room temperature. The formation of G-quadruplex structures was assessed by CD spectroscopy and PAGE under non-denaturing conditions. For high-temperature melting measurements, G4 DNA samples were prepared in the presence of different ligands and used in the assays.

4.4 *CD spectroscopy*

The binding reactions contained 5 μM DNA, 10 mM Tris-HCl (pH 7.4), 0.1 mM EDTA and 100 mM KCl. The CD spectra were recorded in the range 200-400 nm with a scanning speed of 100 nm min^{-1} and a response time of 2 sec at 25 °C using a Jasco spectrophotometer equipped with a temperature controller (having a quartz cell with 1 cm path length). The spectrum shown is the average of three scans. The data was analyzed by using Origin 8.0 software.

4.5 *Fluorescence spectroscopy*

The fluorescence emission spectra were recorded on a Jobin Yvon-Spex Fluoromax 3 fluorimeter (Instruments S. A., Inc.) using a quartz cuvette having a path length of 1 cm. The temperature of

the sample was maintained at 25 °C throughout the assay using a Peltier controller. To the assay buffer (10 mM Tris-HCl, pH 7.4, 0.1 mM EDTA and 100 mM KCl) containing 0.6 μM ligand, 25 μM preformed G4 DNA (3 μl) was added and incubated for 5 min prior to recording of spectrum. The ligands were excited at 330 nm and the emission spectra were recorded in the range 350-550 nm using a slit width of 5 nm. The data was analyzed using the Origin 8.0 software.

4.6 *Fluorescent intercalator displacement assay.*

Thiazole orange displacement assay was conducted by adding the ligand at increasing concentrations to the reaction mixture containing G4 DNA-TO complex (1 μM TO + 0.5 μM G4 DNA). After incubation for 5 min, emission spectra were recorded. In each case, the percentage of TO displacement was calculated from the fluorescence intensity (at λ_{ex} = 501 nm and λ_{em} = 531 nm) using the equation: % TO displacement = 100 - [(F_t/F_0) × 100], where F_t is the fluorescence intensity at each titration point and F_0 is the fluorescence of TO bound to G4 DNA as described [66]. The DC_{50} values were determined from the plot of the fluorescence ligand displaced (%) versus the ligand concentration added. The data was analyzed using the Origin 8.0 software.

4.7 *DNA melting measurements*

The melting measurements were conducted using a Jasco spectrophotometer equipped with a temperature controller with a quartz cell having 1 cm path length. Either G4 DNA alone or G4-DNA plus ligand solutions were placed in a 1 cm quartz cuvette. The CD spectra were recorded over the range 200-400 nm at 20-96 °C with increments of 2 °C/min. Further, ellipticity versus

temperature profiles (melting curves) were plotted (for normalized values) at a wavelength of positive maxima and the T_m was determined. Each trace is the average of at least two scans. A blank sample containing only buffer was treated in the same manner and the value subtracted from the collected data.

4.8 *Polymerase stop assay*

Polymerase stop assay was performed as previously described [67] with slight modifications. Briefly, a single-stranded *c-MYC* DNA template (10 nM) bearing the G-quadruplex forming sequence was mixed with ^{32}P-labeled and cold primers (15 nM) in a Tris-HCl buffer (pH 7.4) containing 5 mM KCl, denatured by heating at 95 °C for 5 min, and then slowly cooled down to room temperature. For *Taq* polymerase reactions in the presence of ligands, an appropriate concentration of ligands was added to the reaction mixture before annealing. The primer extension reactions were performed by mixing annealed substrates with the reaction buffer (5 mM $MgCl_2$, 0.5 mM DTT, 1.5 mg/ml BSA, and 0.2 mM dNTPs) and then incubating it with *Taq* DNA polymerase for 30 min either at 48 or 40 °C. The reactions were stopped by the addition of 10 μL loading dye (95% formamide, 10 mM EDTA, 10 mM NaOH, 0.1% xylene cyanol, 0.1% bromophenol blue). The samples were analyzed using 15% urea denaturing PAGE. The gel was fixed for 30 min in a solution containing 10% acetic acid and 10% methanol. The dried gel was exposed to the phosphorimaging screen prior to acquiring images using the Fuji FLA-5000 phosphorImager.

4.9 Computational studies

The ligands under study were energy optimized using the Gaussian 03 suite program with B3LYP/6-31G* level of theory. The G-quadruplex DNA structures formed by various G-rich promoter sequences, namely PDB 2O3M (*c-KIT*), 2KQH (*c-KIT2*), 2M27 (*VEGF*), 1KF1 (H_{Telo}), 1XAV *(c-MYC*) and 2F8U (*BCL2*), were used in docking studies with the ligands using the AutoDock 4.0 software [64]. A grid box (with dimensions of 126 × 126 × 126 points, spacing = 0.375 Å) was used, keeping the center at the macromolecule. The calculations were performed by utilizing the Lamarckian genetic algorithm (LGA) with a random initial population size = 150 the maximum number of energy evaluations 2500000, the maximum number of generations = 27000 and a mutation rate = 0.02. One hundred independent docking runs were carried out for respective ligands with the root-mean-square (RMS) cut-off set at 0.5 Å.

4.10 RNA isolation and qRT-PCR

The HeLa cells were seeded in 6-well plates and treated with different concentrations of ligand 4. After 24 h of treatment, the RNA was isolated by lysing the cells in 1 ml TRI reagent (Sigma-Aldrich) following instructions provided by the manufacturer. The aqueous phase containing RNA was separated by adding 0.2 ml chloroform followed by centrifugation at 13000 rpm for 10 min at 4 °C. The total RNA was precipitated with absolute isopropanol, washed with 70% ethanol and dissolved in 20 µl RNase free water. To remove genomic DNA contamination from the isolated RNA, the samples were treated with DNase I. The preparation of RNA was free from genomic DNA as assessed by polymerase chain reaction. One µg RNA was subjected for reverse transcription using the iScript cDNA synthesis kit as per the instructions provided by the manufacturer (Bio-Rad Laboratories, CA). The cDNA was quantified using the iTaq universal

SYBR green supermix kit (Bio-Rad Laboratories, CA). GAPDH was used as an internal control for normalization. The forward and reverse primer sequences for amplification of c-MYC were 5′- TGGTTGCTCCATGAGGAGACA-3′ and 5′-GTGGCACCTCTTGAGGACCT-3′ respectively. VEGF was amplified by the forward primer 5′-TGCATTGGAGCCTTGCCTTG-3′ and reverse primer 5′-CGGCTCACCGCCTCGGCTTG-3′. The internal control GAPDH was amplified by the forward primer 5′-CCCCTTCATTGACCTCAACTAC-3′ and reverse the primer 5′-GAGTCCTTCCACGATACCAAAG-3′.

4.11 Cell viability assay:

The HeLa and MCF7 cells in the logarithmic growth-phase were seeded in 48-well culture plates for 24 h and then treated with various concentration of ligand 5. After 72 h incubation, 30 µl MTT reagent (5 mg/ml) was added to each well. After incubation for 4 h., culture medium was removed and then 300 µl of DMSO was added to each well. Cell viability was quantified by measuring photometric absorbance at 570 nm in a Tecan Infinite 200 Pro multi-well plate reader (Tecan Group Ltd, Mannedorf, Switzerland) and i-control 1.10 software (Tecan Group Ltd). The IC_{50} values were derived from nonlinear regression analysis using GraphPad Prism 5 software.

Acknowledgments

The work was partly supported by Grant-in-Aid DBT-IISc Partnership Program for Advanced Research in Biological Sciences and Bio Engineering from the Department of Biotechnology, New Delhi, and J. C. Bose National Fellowship (SR/S2/JCB-25/2005) from the Department of Science and Technology, New Delhi, to KM.

Author contributions

KM and SB conceived and coordinated the study. MHK, BM, SP and AA performed the experiments. All authors analyzed and discussed the data. KM wrote the paper with inputs from all the co-authors. All authors reviewed the results and approved the final version of the manuscript.

Conflict of interest: None.

Abbreviations

CD	Circular dichroism
DMEM	Dulbecco's Modified Eagle's Medium
DMSO	Dimethyl sulfoxide
dsDNA	Double-stranded DNA
FBS	Fetal bovine serum
FI	Fluorescence intensity
FID	Fluorescent intercalator displacement
FRET	Förster resonance energy transfer
hTelo	Human telomeric region
hTERT	Human telomerase reverse transcriptase gene
ODN	Oligodeoxynucleotide
PAGE	Polyacrylamide gel electrophoresis
PBS	Phosphate buffered saline
RT-PCR	Reverse transcription polymerase chain reaction
ssDNA	Single-stranded DNA
T_m	Melting temperature
TO	Thiazole orange

Appendix A. Supplementary data

Supplementary data related to this article can be found at http://

References

[1] S. Burge, G.N. Parkinson, P. Hazel, A.K. Todd, S. Neidle, Quadruplex DNA: sequence, topology and structure, Nucleic Acids Res., 34 (2006), pp. 5402-5415.

[2] Y. Sannohe, H. Sugiyama, Overview of formation of G-quadruplex structures, Curr. Protoc. Nucleic Acid Chem., Chapter 17 (2010) Unit 17 12, pp. 11-17.

[3] Y. Qin, L.H. Hurley, Structures, folding patterns, and functions of intramolecular DNA G-quadruplexes found in eukaryotic promoter regions, Biochimie, 90 (2008), pp. 1149-1171.

[4] J.L. Huppert, S. Balasubramanian, Prevalence of quadruplexes in the human genome, Nucleic Acids Res., 33 (2005), pp. 2908-2916.

[5] V.S. Chambers, G. Marsico, J.M. Boutell, M. Di Antonio, G.P. Smith, S. Balasubramanian, High-throughput sequencing of DNA G-quadruplex structures in the human genome, Nat. Biotechnolo., 33 (2015), pp. 877-881.

[6] D. Rhodes, H.J. Lipps, G-quadruplexes and their regulatory roles in biology, Nucleic Acids Res., 43 (2015), pp. 8627-8637.

[7] J.L. Huppert, S. Balasubramanian, G-quadruplexes in promoters throughout the human genome, Nucleic Acids Res., 35 (2007), pp. 406-413.

[8] D. Sun, L.H. Hurley, The importance of negative superhelicity in inducing the formation of G-quadruplex and i-motif structures in the c-Myc promoter: implications for drug targeting and control of gene expression, J. Med. Chem., 52 (2009), pp. 2863-2874.

[9] C. Zhang, H.H. Liu, K.W. Zheng, Y.H. Hao, Z. Tan, DNA G-quadruplex formation in response to remote downstream transcription activity: long-range sensing and signal transducing in DNA double helix, Nucleic Acids Res., 41 (2013), pp. 7144-7152.

[10] G. Biffi, D. Tannahill, J. McCafferty, S. Balasubramanian, Quantitative visualization of DNA G-quadruplex structures in human cells, Nat. Chem., 5 (2013), pp. 182-186.

[11] G. Biffi, M. Di Antonio, D. Tannahill, S. Balasubramanian, Visualization and selective chemical targeting of RNA G-quadruplex structures in the cytoplasm of human cells, Nat. Chem., 6 (2014) 75-80.

[12] A. Henderson, Y. Wu, Y.C. Huang, E.A. Chavez, J. Platt, F.B. Johnson, R.M. Brosh, Jr., D. Sen, P.M. Lansdorp, Detection of G-quadruplex DNA in mammalian cells, Nucleic Acids Res., 42 (2014), pp. 860-869.

[13] T. de Lange, Shelterin: the protein complex that shapes and safeguards human telomeres, Genes Dev., 19 (2005), pp. 2100-2110.

[14] W. Palm, T. de Lange, How shelterin protects mammalian telomeres, Ann. Rev. Genet., 42 (2008), pp. 301-334.

[15] C.W. Greider, E.H. Blackburn, Identification of a specific telomere terminal transferase activity in Tetrahymena extracts, Cell, 43 (1985), pp. 405-413.

[16] S.B. Cohen, M.E. Graham, G.O. Lovrecz, N. Bache, P.J. Robinson, R.R. Reddel, Protein composition of catalytically active human telomerase from immortal cells, Science, 315 (2007), pp. 1850-1853.

[17] J.W. Shay, W.E. Wright, Telomerase: a target for cancer therapeutics, Cancer cell, 2 (2002), pp. 257-265.

[18] D. Yang, K. Okamoto, Structural insights into G-quadruplexes: towards new anticancer drugs, Future Med. Chem., 2 (2010), pp. 619-646.

[19] A. Ambrus, D. Chen, J. Dai, T. Bialis, R.A. Jones, D. Yang, Human telomeric sequence forms a hybrid-type intramolecular G-quadruplex structure with mixed parallel/antiparallel strands in potassium solution, Nucleic Acids Res., 34 (2006), pp. 2723-2735.

[20] G.N. Parkinson, M.P. Lee, S. Neidle, Crystal structure of parallel quadruplexes from human telomeric DNA, Nature, 417 (2002), pp. 876-880.

[21] Y. Wang, D.J. Patel, Solution structure of the human telomeric repeat d[AG3(T2AG3)3] G-tetraplex, Structure, 1 (1993), pp. 263-282.

[22] Y. Xu, Y. Noguchi, H. Sugiyama, The new models of the human telomere d[AGGG(TTAGGG)3] in K+ solution, Bioorg. Med. Chem., 14 (2006), pp. 5584-5591.

[23] K.N. Luu, A.T. Phan, V. Kuryavyi, L. Lacroix, D.J. Patel, Structure of the human telomere in K+ solution: an intramolecular (3 + 1) G-quadruplex scaffold, J. Am. Chem. Soc., 128 (2006), pp. 9963-9970.

[24] S. Balasubramanian, L.H. Hurley, S. Neidle, Targeting G-quadruplexes in gene promoters: a novel anticancer strategy?, Nature Rev. Drug Disco., 10 (2011), pp. 261-275.

[25] Q. Li, J.F. Xiang, Q.F. Yang, H.X. Sun, A.J. Guan, Y.L. Tang, G4LDB: a database for discovering and studying G-quadruplex ligands, Nucleic Acids Res., 41 (2013), pp. 1115-1123.

[26] T.A. Brooks, S. Kendrick, L. Hurley, Making sense of G-quadruplex and i-motif functions in oncogene promoters, FEBS J., 277 (2010), pp. 3459-3469.

[27] M.C. Hammond-Kosack, B. Dobrinski, R. Lurz, K. Docherty, M.W. Kilpatrick, The human insulin gene linked polymorphic region exhibits an altered DNA structure, Nucleic Acids Res., 20 (1992), pp. 231-236.

[28] A. Siddiqui-Jain, C.L. Grand, D.J. Bearss, L.H. Hurley, Direct evidence for a G-quadruplex in a promoter region and its targeting with a small molecule to repress c-MYC transcription, Proc. Natl. Acad. Sci. U. S. A., 99 (2002), pp. 11593-11598.

[29] D. Sun, K. Guo, J.J. Rusche, L.H. Hurley, Facilitation of a structural transition in the polypurine/polypyrimidine tract within the proximal promoter region of the human VEGF gene by the presence of potassium and G-quadruplex-interactive agents, Nucleic Acids Res., 33 (2005), pp. 6070-6080.

[30] R. De Armond, S. Wood, D. Sun, L.H. Hurley, S.W. Ebbinghaus, Evidence for the presence of a guanine quadruplex forming region within a polypurine tract of the hypoxia inducible factor 1alpha promoter, Biochemistry, 44 (2005), pp. 16341-16350.

[31] T.S. Dexheimer, D. Sun, L.H. Hurley, Deconvoluting the structural and drug-recognition complexity of the G-quadruplex-forming region upstream of the bcl-2 P1 promoter, J. Am. Chem. Soc., 128 (2006), pp. 5404-5415.

[32] A. Yafe, S. Etzioni, P. Weisman-Shomer, M. Fry, Formation and properties of hairpin and tetraplex structures of guanine-rich regulatory sequences of muscle-specific genes, Nucleic Acids Res., 33 (2005), pp. 2887-2900.

[33] S. Cogoi, L.E. Xodo, G-quadruplex formation within the promoter of the KRAS proto-oncogene and its effect on transcription, Nucleic Acids Res., 34 (2006), pp. 2536-2549.

[34] S. Rankin, A.P. Reszka, J. Huppert, M. Zloh, G.N. Parkinson, A.K. Todd, S. Ladame, S. Balasubramanian, S. Neidle, Putative DNA quadruplex formation within the human c-kit oncogene, J. Am. Chem. Soc., 127 (2005), pp. 10584-10589.

[35] K. Guo, A. Pourpak, K. Beetz-Rogers, V. Gokhale, D. Sun, L.H. Hurley, Formation of pseudosymmetrical G-quadruplex and i-motif structures in the proximal promoter region of the RET oncogene, J. Am. Chem. Soc., 129 (2007), pp. 10220-10228.

[36] Y. Qin, E.M. Rezler, V. Gokhale, D. Sun, L.H. Hurley, Characterization of the G-quadruplexes in the duplex nuclease hypersensitive element of the PDGF-A promoter and modulation of PDGF-A promoter activity by TMPyP4, Nucleic Acids Res., 35 (2007), pp. 7698-7713.

[37] M. Kaulage, B. Maji, J. Bhat, Y. Iwasaki, S. Chatterjee, S. Bhattacharya, K. Muniyappa, Discovery and structural characterization of G-quadruplex DNA in human acetyl-CoA carboxylase gene promoters: its role in transcriptional regulation and as a therapeutic target for human disease, J. Med. Chem., 59 (2016), pp. 5035-5050.

[38] Y. Chen, D. Yang, Sequence, stability, and structure of G-quadruplexes and their interactions with drugs, Curr. Protoc. Nucleic Acid Chem., Chapter 17 (2012) Unit17, pp. 15.

[39] D. Monchaud, M.P. Teulade-Fichou, A hitchhiker's guide to G-quadruplex ligands, Org. Biomol. Chem., 6 (2008), pp. 627-636.

[40] B. Maji, S. Bhattacharya, Advances in the molecular design of potential anticancer agents via targeting of human telomeric DNA, Chem. Commun., 50 (2014), pp. 6422-6438.

[41] A. Arola, R. Vilar, Stabilisation of G-quadruplex DNA by small molecules, Curr. Top. Med. Chem., 8 (2008), pp. 1405-1415.

[42] B. Maji, K. Kumar, M. Kaulage, K. Muniyappa, S. Bhattacharya, Design and synthesis of new benzimidazole-carbazole conjugates for the stabilization of human telomeric DNA, telomerase inhibition, and their selective action on cancer cells, J. Med. Chem., 57 (2014), pp. 6973-6988.

[43] B. Maji, K. Kumar, K. Muniyappa, S. Bhattacharya, New dimeric carbazole-benzimidazole mixed ligands for the stabilization of human telomeric G-quadruplex DNA and as telomerase inhibitors. A remarkable influence of the spacer, Org. Biomol. Chem., 13 (2015), pp. 8335-8348.

[44] M. Hranjec, G. Pavlovic, M. Marjanovic, M. Kralj, G. Karminski-Zamola, Benzimidazole derivatives related to 2,3-acrylonitriles, benzimidazo[1,2-a]quinolines and fluorenes: synthesis, antitumor evaluation in vitro and crystal structure determination, Eur. J. Med. Chem., 45 (2010), pp. 2405-2417.

[45] C.G. Neochoritis, T. Zarganes-Tzitzikas, C.A. Tsoleridis, J. Stephanidou-Stephanatou, C.A. Kontogiorgis, D.J. Hadjipavlou-Litina, T. Choli-Papadopoulou, One-pot microwave assisted synthesis under green chemistry conditions, antioxidant screening, and cytotoxicity assessments of benzimidazole Schiff bases and pyrimido[1,2-a]benzimidazol-3(4H)-ones, Eur. J. Med. Chem., 46 (2011), pp. 297-306.

[46] S. Demirayak, I. Kayagil, L. Yurttas, Microwave supported synthesis of some novel 1,3-diarylpyrazino[1,2-a]benzimidazole derivatives and investigation of their anticancer activities, Eur. J. Med. Chem., 46 (2011), pp. 411-416.

[47] C. Bailly, G. Chessari, C. Carrasco, A. Joubert, J. Mann, W.D. Wilson, S. Neidle, Sequence-specific minor groove binding by bis-benzimidazoles: water molecules in ligand recognition, Nucleic Acids Res., 31 (2003), pp. 1514-1524.

[48] Y. Bansal, O. Silakari, The therapeutic journey of benzimidazoles: a review, Bioorg. Med. Chem., 20 (2012), pp. 6208-6236.

[49] Q.a.Y. Zhou, P., Crystal structure and DNA-binding studies of a new Cu(II) complex involving benzimidazole, Inorg. Chim. Acta., 359 (2006), pp. 1200-1206.

[50] A.K. Jain, S. Bhattacharya, Interaction of G-quadruplexes with nonintercalating duplex-DNA minor groove binding ligands, Bioconjug. Chem., 22 (2011), pp. 2355-2368.

[51] K. Thevissen, A. Marchand, P. Chaltin, E.M. Meert, B.P. Cammue, Antifungal carbazoles, Curr. Med. Chem., 16 (2009), pp. 2205-2211.

[52] H.J. Knolker, K.R. Reddy, Chemistry and biology of carbazole alkaloids, The Alkaloids. Chem. Bio., 65 (2008), pp. 1-410.

[53] C. Asche, M. Demeunynck, Antitumor carbazoles, Anti-cancer Agents Med. Chem., 7 (2007), pp. 247-267.

[54] M. Bashir, A. Bano, A.S. Ijaz, B.A. Chaudhary, Recent developments and biological activities of N-substituted carbazole derivatives: a review, Molecules, 20 (2015), pp. 13496-13517.

[55] A. Gluszynska, Biological potential of carbazole derivatives, Eur. J. Med. Chem., 94 (2015), pp. 405-426.

[56] C.C. Chang, J.Y. Wu, C.W. Chien, W.S. Wu, H. Liu, C.C. Kang, L.J. Yu, T.C. Chang, A fluorescent carbazole derivative: high sensitivity for quadruplex DNA, Anal. Chem., 75 (2003), pp. 6177-6183.

[57] T.C. Chang, C.C. Chang, Detection of G-quadruplexes in cells and investigation of G-quadruplex structure of d(T2AG3)4 in K+ solution by a carbazole derivative: BMVC, Methods Mol. Biol., 608 (2010), pp. 183-206.

[58] W.J. Chen, C.X. Zhou, P.F. Yao, X.X. Wang, J.H. Tan, D. Li, T.M. Ou, L.Q. Gu, Z.S. Huang, Disubstituted 1,8-dipyrazolcarbazole derivatives as a new type of c-myc G-quadruplex binding ligands, Bioorg. Med. Chem., 20 (2012), pp. 2829-2836.

[59] D. Lin, X. Fei, Y. Gu, C. Wang, Y. Tang, R. Li, J. Zhou, A benzindole substituted carbazole cyanine dye: a novel targeting fluorescent probe for parallel c-myc G-quadruplexes, Analyst, 140 (2015), pp. 5772-5780.

[60] T.Y. Tse, C.C. Chang, J.J. Lin, T.C. Chang, A fluorescent anti-cancer agent, 3,6-bis(1-methyl-4-vinylpyridinium) carbazole diiodide, stains G-quadruplexes in cells and inhibits tumor growth, Curr. Top. Med. Chem., 15 (2015), pp. 1964-1970.

[61] J. Kypr, I. Kejnovska, D. Renciuk, M. Vorlickova, Circular dichroism and conformational polymorphism of DNA, Nucleic Acids Res., 37 (2009), pp. 1713-1725.

[62] Y. Xue, Z.Y. Kan, Q. Wang, Y. Yao, J. Liu, Y.H. Hao, Z. Tan, Human telomeric DNA forms parallel-stranded intramolecular G-quadruplex in K+ solution under molecular crowding condition, J. Am. Chem. Soc., 129 (2007), pp. 11185-11191.

[63] D. Monchaud, C. Allain, M.P. Teulade-Fichou, Development of a fluorescent intercalator displacement assay (G4-FID) for establishing quadruplex-DNA affinity and selectivity of putative ligands, Bioorg. Med. Chem. Lett., 16 (2006), pp. 4842-4845.

[64] G.M.G. Morris, D. S.; Halliday, R. S.; Huey, R.; Hart, W. E.; Belew, R. K. and Olson, A. J., Automated docking using a Lamarckian genetic algorithm and an empirical binding free energy function, J. Comput. Chem., 19 (1998), pp. 1639−1662.

[65] J. Reed, M. Gunaratnam, M. Beltran, A.P. Reszka, R. Vilar, S. Neidle, TRAP-LIG, a modified telomere repeat amplification protocol assay to quantitate telomerase inhibition by small molecules, Anal. Biochem., 380 (2008), pp. 99-105.

[66] D. Monchaud, C. Allain, H. Bertrand, N. Smargiasso, F. Rosu, V. Gabelica, A. De Cian, J.L. Mergny, M.P. Teulade-Fichou, Ligands playing musical chairs with G-quadruplex DNA: a rapid and simple displacement assay for identifying selective G-quadruplex binders, Biochimie, 90 (2008), pp. 1207-1223.

[67] H. Han, L.H. Hurley, M. Salazar, A DNA polymerase stop assay for G-quadruplex-interactive compounds, Nucleic Acids Res., 27 (1999), pp. 537-542.

Table 1

Promoter	5'<-----Sequence----->3'
C-Myc	TGGGGAGGGTGGGGAGGGTGGGGAAGG
VEGF	CGGGGCGGGCCGGGGGCGGGGT
Telomere	TTAGGGTTAGGGTTAGGGTTAGGG
c-Kit	AGGGAGGGCGCTGGGAGGAGGG
c-Kit-2	CGGGCGGGCGCGAGGGAGGGG
BCL2	AGGGGCGGGCGCGGGAGGAAGGGGGCGGGAGCGGGGCTG

Table 2

Ligand	DC_{50} (μM)						
	Telomere	*c-MYC*	*BCL2*	*c-KIT1*	*c-KIT2*	*VEGF*	*ct-DNA*
1	2.79	1.63	2.86	1.62	1.34	1.42	5.28
2	1.30	0.85	1.29	0.98	0.74	0.63	5.52
3	>3	>3	>3	>3	>3	>3	>10
4	1.15	0.98	1.44	0.88	0.66	0.75	6.49
5	1.13	0.83	1.39	0.86	0.65	0.78	6.94
TMPyP4	0.47	0.38	0.43	0.32	0.35	0.31	0.87

Table 3

Ligand	ΔT_m (°C)					
	Telomere	*c-MYC*	*BCL2*	*c-KIT1*	*c-KIT2*	*VEGF*
1	9.74	8.63	6.53	13.18	17.00	12.79
2	16.86	8.65	5.54	12.20	16.55	14.18
3	7.14	4.95	3.26	3.58	7.53	4.35
4	21.17	8.86	9.50	25.88	21.96	14.15
5	21.26	7.35	9.54	24.69	23.27	11.28
TMPyP4	15.63	10.97	14.27	15.14	15.54	12.35